---

**Article:**
Yildiz, V. orcid.org/0000-0001-5146-2684, Brown, S. orcid.org/0000-0001-8229-8004 and Rougé, C. (2025) Robust and computationally efficient design for run-of-river hydropower. Environmental Modelling & Software, 183. 106220. ISSN 1364-8152

https://doi.org/10.1016/j.envsoft.2024.106220

---

Environmental Modelling and Software 183 (2025) 106220

Contents lists available at ScienceDirect

Environmental Modelling and Software

journal homepage: www.elsevier.com/locate/envsoft

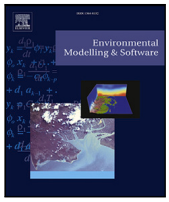

# Robust and computationally efficient design for run-of-river hydropower

Veysel Yildiz [a,*], Solomon Brown [b], Charles Rougé [a]

[a] Department of Civil and Structural Engineering, The University of Sheffield, Sheffield, United Kingdom
[b] Department of Chemical and Biological Engineering, The University of Sheffield, Sheffield, United Kingdom

ARTICLE INFO

Dataset link: https://doi.org/10.15131/shef.data.25676967.v1, https://github.com/Veysel-Yildiz/Robust-and-computationally-efficient-Design-for-RoR-the-HYPER-FORD

*Keywords:*
RoR hydropower
HYPER
MORDM

ABSTRACT

This paper introduces innovative approaches for robust and computationally efficient optimal design of run-of-river hydropower plants. Compared with existing design software, it (1) integrates optimized turbine operations into design optimization instead of following predefined operational rules, and (2) combines this with a regular sampling of the flow duration curve to significantly reduce data inputs. Our rigorous benchmarking demonstrates that (1) operation optimization improves design performance at low computational cost, whilst (2) data input reduction slashes computational costs by over 92% with minimal impact on design recommendations and key robustness analysis insights. Taken together, these innovations make integrated design and operation optimization, complete with in-depth robustness analysis, laptop-accessible. They also reinforce sustainability efforts by minimizing the need for high-performance computing and large associated embodied greenhouse gas emissions.

## 1. Introduction

Small hydropower plants (SHPs) offer an environmentally friendly and cost-effective alternative to conventional dam-based plants (Tsuanyo et al., 2023). While only 36% of their global potential is currently tapped (UNIDO, 2022), a significant global expansion is expected (Couto and Olden, 2018), including in industrial nations where the best sites for large-scale hydropower are already taken such as Europe (Kuriqi et al., 2020; Kishore et al., 2021). The majority of SHPs follow the run-of-the-river (RoR) scheme (Yildiz and Vrugt, 2019), relying on the dynamic flow of rivers for hydropower generation due to their sub-daily storage capacity. Out of over 3,000 power plants of 1 MW capacity or more, either planned or under construction, notably in emerging economies (Zarfl et al., 2015), RoR plants account for more than 75% of the total (Bejarano et al., 2019). This momentum ensures that hydropower will remain a key electricity supply source globally in decades to come (Winemiller et al., 2016; Gernaat et al., 2017; Pokhrel et al., 2018; Moran et al., 2018). It also aligns with the seventh Sustainable Development Goal (SDG) of providing affordable, dependable, sustainable, and modern energy for all (McCollum et al., 2017; Dorber et al., 2020), whilst contributing to other SDG targets (Gielen et al., 2019).

RoRs designed today will be deployed in a world characterized by a changing climate and uncertain economic conditions. Observations from the Global Precipitation Climatology Center (Spinoni et al., 2014) and recent studies (Spinoni et al., 2018; Ault, 2020; Sreeparvathy and Srinivas, 2022; Yildiz et al., 2022; Fang et al., 2022) highlight increasing global trends in the frequency, length, and intensity of meteorological droughts. These trends could directly lead to increases in streamflow drought in the future over a wide range of climate zones in tropical and temperate regions (Cook et al., 2020; Zhang et al., 2023). RoR schemes lack the storage capacity to regulate seasonal discharge fluctuations, making them significantly more vulnerable to these changes than plants sited at the outlet of large reservoirs. Climate risks are compounded by the risks that socio-economic uncertainty also pose to the long-term viability of hydropower projects, and both should be considered simultaneously in project development (Shaktawat and Vadhera, 2021). In fact, there are documented examples of socio-economic risks being a more critical future uncertainty for the performance of a hydropower investment than climate change (Ray et al., 2018; Yildiz et al., 2024). These studies stress the importance of an integrated evaluation of the potential impacts of these uncertainties on the financial viability of hydropower investments as early as the planning phase.

Besides integrating uncertainty, hydropower plant design should also explicitly incorporate optimized operations. Yet, that is often not the case for RoR plant design where ad hoc operational rules are considered instead, primarily for computational simplicity (e.g., Anagnostopoulos and Papantonis, 2007; Mamo et al., 2018; Yildiz et al., 2024). However, there is evidence that design and operation of hydropower infrastructure could be critically dependent on each other, including in

* Corresponding author.
*E-mail addresses:* vyildiz1@sheffield.ac.uk (V. Yildiz), s.f.brown@sheffield.ac.uk (S. Brown), c.rouge@sheffield.ac.uk (C. Rougé).

https://doi.org/10.1016/j.envsoft.2024.106220
Received 27 April 2024; Received in revised form 20 August 2024; Accepted 16 September 2024
Available online 19 September 2024

situations where there is a need to address hydro-climatic variability, climate change and unintended consequences of development (Bertoni et al., 2019). To address this and achieve future-proof planning where investments remain financially resilient to perturbations, design and operations should be robust, i.e., able to withstand deviations from design conditions (Herman et al., 2015). Numerous frameworks (e.g., Lempert, 2002; Bryant and Lempert, 2010; Brown et al., 2012; Haasnoot et al., 2013; Kasprzyk et al., 2013) have been developed in recent years to integrate considerable future uncertainties and assess their impact on design, operations and adaptation in complex (water) infrastructure systems. Beside a common focus on robustness, they recognize that the multi-stakeholder, multi-purpose nature of these systems, combined with unquantifiable future uncertainty, lead to deep uncertainty (Kwakkel et al., 2016), whereby formulating the problem and its boundaries becomes a challenge in itself.

In water resource systems that include complex interactions between design variables and operation restrictions, both multi-objective optimization and robustness analysis typically demand a substantial amount of computing time and resources. These computational requirements become even more pronounced when conducting exploratory studies involving both steps (e.g., Quinn et al., 2018; Bertoni et al., 2019). They then create a need for large-scale computing solutions — High-Performance Computing (HPC) or cloud-based computing, and contributes significantly to the increasing need for large-scale computing solutions, including supercomputers and data centers (Hussain et al., 2019; Lannelongue et al., 2021). In turn, this quest for enhanced processing capacity raises environmental concerns (Hernandez et al., 2018; Katal et al., 2023), because the electricity that needs to be mobilized for the continuous use of computational facilities contributes to climate change, resource depletion, and strain on local power infrastructures (Bharany et al., 2022). Thus, scientific and large-scale technical computing presently account for 0.3% of global carbon emissions, and this share is likely to increase in the future (Jones, 2018; Cao et al., 2022; Katal et al., 2022), creating an additional, considerable challenge to global climate change mitigation measures. As the need for large-scale computing grows, finding innovative technical solutions that balance these computing demands with energy economy and environmental responsibility becomes critical. These solutions will also remove barriers to application of these methods beyond actors in industrialized nations – academia and corporations – that often lack the human and physical infrastructure to use the most largest computing facilities.

This study proposes approximations to slash the computational requirements associated with the robust design of RoR hydropower plants, to (1) make robust design and analysis more accessible thereby accelerating decision-making processes significantly, and to (2) reinforce sustainability efforts by reducing dependence on high-performance computing and mitigating carbon emissions from data centers. It aims to do this without compromising accuracy and in fact, by explicitly incorporating optimized operations into design for the first time. These two innovations, together, lead to Fast Operation-optimized Robust Design of run-of-river HYdroPowER plants, summarized by the acronym HYPER-FORD that we will use throughout this paper.

The methodological steps employed in this paper, which also dictate its organization, are provided in Fig. 1. In Section 2, we summarize the robust RoR hydropower design approach introduced in Yildiz et al. (2024) which is our starting point for this paper. This is followed by the introduction of the case studies used to benchmark the innovations included in this work. Section 3 then introduces HYPER-FORD and its two key innovations; (3.1) HYPER$_{OP}$ module for coupled design and operation optimization and (3.2) a discretization of the flow duration curve (FDC) to strategically reduce data input and enhance computational efficiency. Following this, in Section 4, we detail the methodology for benchmarking our innovations. Benchmarking results in Section 5 then validate these innovations. Lastly, in Section 6, we discuss the broader implications of our results, explore opportunities for future research, and conclude this paper with a summary of our main findings.

## 2. Robust design: HYPER-MORDM framework

From this point on, we call HYPER-MORDM the analytical framework developed in Yildiz et al. (2024) that merges the Many Objective Robust Decision Making (MORDM) approach (Kasprzyk et al., 2013) with the versatile capabilities of the HYPER toolbox (Yildiz and Vrugt, 2019). HYPER is a state-of-the-art RoR plant design toolbox that identifies optimal design parameters for user-selected power production or financial performance metrics. As depicted in the upper gray box in Fig. 1, the HYPER-MORDM comprises of two main steps: design optimization with multiple financial objectives (Section 2.1) and robustness analysis (Section 2.2).

A key element in both stages of HYPER-MORDM in the use of FDCs, defined as cumulative frequency curves depicting streamflow (e.g., at a planned RoR plant site) as a function of percentage of time discharge is equaled or exceeded within a specified climate state (Vogel and Fennessey, 1994). A FDC represent the full range of hydrological conditions available at a catchment's outlet (Yilmaz et al., 2008; Sadegh et al., 2016). It serves as an essential tool in the design of small hydropower systems including RoRs (Basso and Botter, 2012; Yildiz and Vrugt, 2019). FDCs are serving not only during optimization purposes, but also as a basis for synthetically generating plausible futures for robustness analysis (Yildiz et al., 2023). We now describe in detail the two main steps of HYPER-MORDM.

### 2.1. Design optimization

HYPER-MORDM conducts design optimization based on financial performance metrics that rely on lifetime expected net present benefits and costs. The lifetime expected net present revenues from hydropower production are given by:

$$\mathrm{R} = \sum_{y=1}^{L_s} \frac{R_y}{(1+r_y)^y} \tag{1}$$

where $L_s$ is the project's lifetime, typically 50 years, and $\mathbf{R} = \{R_1 \ldots, R_{L_s}\}$ and $\mathbf{r} = \{r_1, \ldots, r_{L_s}\}$ are vectors of length $L_s$ of the annual plant revenues assuming an average hydropower production throughout the year (by default in USD) and the annual interest (discount) rate in %, respectively. Similarly, the lifetime net present cost of a RoR hydropower plant design, which significantly depends on site-specific factors, can be expressed as:

$$\mathrm{C} = C_{\mathrm{Tp}} + \frac{C_{\mathrm{Rem}}}{(1+r_{HL})^{HL}} + \sum_{y=1}^{L_s} \frac{C_{\mathrm{om}}}{(1+r_y)^y} \tag{2}$$

where $C_{\mathrm{Tp}}$ is the investment cost, $C_{\mathrm{Rem}}$ is the renovation and reconstruction cost of electro-mechanic equipment at year $HL$ halfway through the plant's lifetime, typically at year 25, and $C_{\mathrm{om}}$ is the yearly maintenance and operation cost. Each component of benefit and cost equations is discussed in detail in Yildiz and Vrugt (2019).

Net present revenue and cost can be combined into the net present value (NPV), defined as the value of projected cash flows discounted to the present (Santolin et al., 2011):

$$f_{\mathrm{NPV}} = R - C \tag{3}$$

They can also be combined into a ratio, the benefit–cost ratio (BC):

$$f_{\mathrm{BC}} = \frac{R}{C} \tag{4}$$

Whereas NPV focuses on the expected profit, the BC focuses on the risk of the projects (Anagnostopoulos and Papantonis, 2007; Basso and Botter, 2012). Thus, maximizing the NPV leads to a design that offers the highest return, whereas maximizing the BC would result in design with lower investment costs compared with expected revenue, and therefore diminished financial risks.

The HYPER-MORDM framework allows both single and double objective formulation using $f_{\mathrm{NPV}}$ and $f_{\mathrm{BC}}$ as design objectives. The two

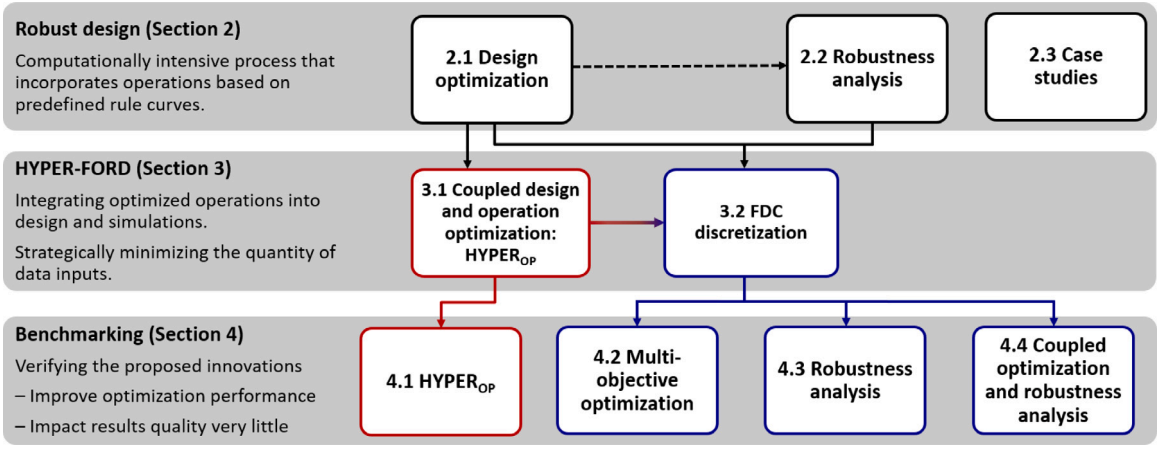


**Fig. 1.** Flowchart outlining methodological steps for developing our computationally inexpensive robust design approach.

objective formulation enables the user to trade-off the most commonly used traditional design objective (NPV) with another financial objective assumed to be more focused on project risks:

$$F(x) = \max[\, f_{\mathrm{NPV}},\ f_{\mathrm{BC}}] \tag{5}$$

where $x$ is the vector of decision variables including all the key design parameters such as turbine type, turbine number, turbine's installed capacities, penstock diameter. In this approach, we employ simulation optimization to compute energy generation for each day of a multi-decadal flow record, represented by its FDC. Using daily multidecadal flow records is standard practice in simulation optimization of water resource systems (e.g., Quinn et al., 2018; Bertoni et al., 2019).

### 2.2. Robustness analysis

The HYPER-MORDM approach involves evaluating the performance of alternatives identified during optimization across a range of plausible futures. This implies defining ranges for relevant parameters, then sampling an appropriate number of plausible climatic and socio-economic futures. In particular, sampled hydro-climatic parameters are used to derive FDCs (Yildiz et al., 2023). In Panel A of Fig. 2 (adapted from Yildiz et al.), the blue line represents the FDC of long-term historical observations at a possible development site in Turkey, while the gray lines depict plausible future FDCs across a range of drier and more variable futures. The generated futures reflect the expected drying and increased variability anticipated in the region due to climate change. Each sampled FDC is disaggregated into 50 long-term time series of daily discharge values generated using the Kirsch-Nowak streamflow generator developed by Quinn et al. (2017), to model the natural variability of each climate (Panel B in Fig. 2).

These flows are then used for robustness quantification. Each time series' duration aligns with the typical licensing duration of a RoR hydropower project in the jurisdiction where a project is being considered. The HYPER-MORDM approach focuses on financial robustness based on two key financial viability metrics, (1) the payback period (PB) and (2) NPV. The PB, is a metric that shows the length of time required to recover capital investments, is computed as;

$$PB = \frac{C_{Tp}}{\overline{R} - C_{om}} \tag{6}$$

where $C_{Tp}$ the investment cost defined in Eq. (2), and the denominator is the project's expected amount of annual net cash inflow.

Both NPV and PB metrics form the basis of robustness metrics based on satisficing criteria (Herman et al., 2015) by comparing their values to desirability thresholds. Satisficing criteria are particularly well-suited for RoR hydropower projects, as they enable decision-makers to identify solutions that meet acceptable financial performance thresholds across multiple objectives. Unlike regret analysis or scenario-based optimization, which focus on minimizing regret or maximizing expected performance, satisficing metrics are easily interpretable. Even though results depend heavily on the choice of thresholds (McPhail et al., 2018) those can be user-defined, and it should be noted that the choice of a non-satisficing robustness metric among several choices also heavily influences robustness assessments (Giuliani and Castelletti, 2016). Typically, small hydropower projects are deemed viable when the PB is below 15 years (Alonso-Tristán et al., 2011; Girma, 2016; Ak et al., 2017). Consequently, for each of the 50 time series defined for each plausible future, we establish robustness using PB as a binary variable:

$$\mathrm{RM}_k = \begin{cases} 0, & \mathrm{PB} > 15; \text{years} \\ 1, & \mathrm{PB} \le 15; \text{years} \end{cases} \tag{7}$$

Success is attributed to each plausible future if, for at least 75% of the time series (i.e., 38 or more out of 50), $RM_k$ is confirmed to be 1. The binary variables are also aggregated across all realizations of all plausible future to create an average robustness score, denoted as $RM_{\mathrm{PB}}$.

We use a similar approach to calculate the robustness metric based on NPV, $RM_{\mathrm{NPV}}$. For each of the 50 time series we define robustness as a binary variable:

$$\mathrm{RM}_k = \begin{cases} 0, & \mathrm{NPV} > 0 \\ 1, & \mathrm{NPV} \le 0 \end{cases} \tag{8}$$

Then, we define a future as success or failure depending on whether NPV> 0 over 75% of the time. Alternatively, we aggregate over all 50 time series over all futures to compute $RM_{\mathrm{NPV}}$. In-depth rationale of the determination of objective functions and derivation of robustness metrics are available in Yildiz et al. (2024).

### 2.3. Case studies: physical characteristics and uncertainties

This subsection introduces the case studies to which the HYPER-MORDM approach and the innovations introduced in this paper are applied, including how climatic and socio-economic uncertainties are considered. Detailed information on the case studies and a comprehensive justification for the robustness analysis, including all uncertain parameters and their associated sampling ranges, is provided in Yildiz et al. (2024).

#### 2.3.1. Case studies description

We consider five proposed RoR hydropower plants in Turkey (Yildiz et al., 2024). The top panel of Fig. 3 (adapted from Yildiz et al.) illustrates the diverse hydro-climatic settings of the five case studies,

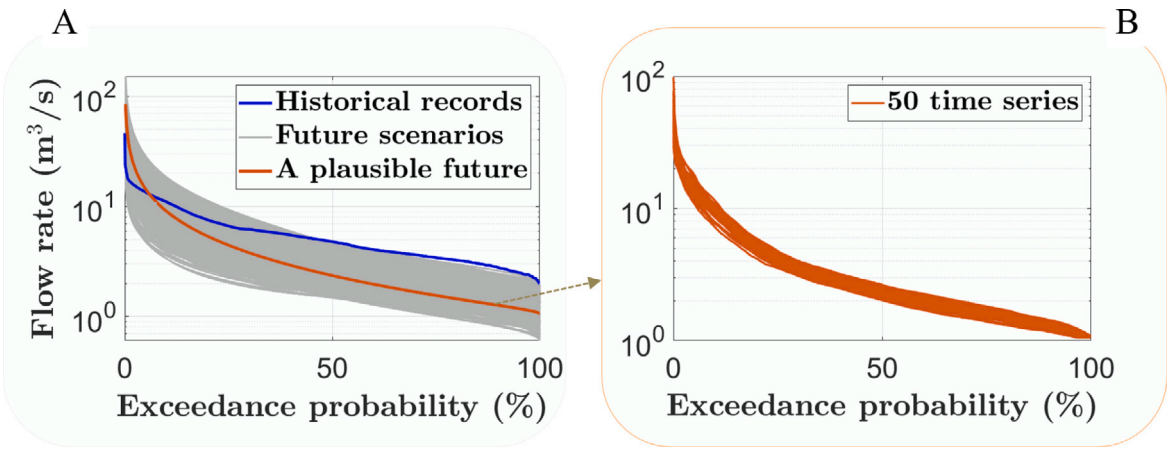


**Fig. 2.** Panel A: Plot of the flow duration curves (FDC) of observed discharge (blue line), future flows (gray lines) and a random future (orange color). Panel B: Desegregation of the selected future (orange color) to 50 time series (orange lines). The $X$-axis denotes the exceedance probability, while the $Y$-axis logarithmically scales the flow rate.

as indicated by the Köppen–Geiger climate classification based on four high-resolution climatic maps spanning from 1980 to 2016 (Beck et al., 2018). Besik and Kaplan RoRs have a Mediterranean-influenced humid continental climate, while Buyukdere RoR experiences a humid continental climate. Tepe RoR is situated in a humid subtropical climate area, and Karacay RoR falls under the Mediterranean climate. Table 1 summarizes the site and streamflow characteristics of these case-studies. The coefficient of variation (CV) represents the ratio of the mean to the standard deviation of the daily streamflow time series, and different values reflect the distinct hydrological and hydro-climatic conditions across our catchments. This variability is further highlighted in Table 1, which presents a range from 1 to 6 in mean flows and demonstrates a threefold difference between the highest and lowest values of the coefficient of variation (CV) across the sites. Cross-catchment variations in precipitation patterns and watershed attributes such as land use, soil type, and slope contribute to distinct hydrological features, are also evident through the normalized FDCs in the bottom panel of Fig. 3. In-depth descriptions of the case studies, including climatic aspects, are available in Yildiz et al. (2024). Table 1 also shows the fraction of river discharge designated for maintaining minimum environmental flow and supporting ecosystem services, as regulated by state authorities. Finally, the table shows the gross hydraulic head available at each site, and the gross potential annual average energy (GAAE) of each site, computed by taking into consideration the available gross head or water pressure, and average long-term discharge. Note that this calculation ignores frictional and minor losses, the influence of flow variability on turbine efficiency, and the fact that flows exceeding the design discharge capacity do not produce hydropower.

Most of the precipitation at Besik, Kaplan, and Buyukdere hydro sites occurs as snow during winter. The snowpack at these locations serves as a natural reservoir, ensuring a steady water supply during the drier summer months. This results in less variability in low-flow ranges compared to the other two sites. Additionally, Besik and Kaplan RoRs boast the highest potential energy, as indicated in Table 1. These catchments' capacity to store precipitation typically reflects in a gradual slope in the middle portion of the FDC (Yilmaz et al., 2008), with Besik exhibiting the mildest slope among the cases. Among all the sites the Besik RoR is anticipated to be the most profitable according to traditional assessments of RoR plants. Therefore, this site will be used for all benchmarking steps, whereas the other four sites will be used primarily to verify that the full HYPER-FORD hydropower design workflow introduced in this paper works as intended.

#### 2.3.2. Plausible futures

Seven uncertain factors are defined and these deeply uncertain factors are assigned sampling ranges to each, as summarized in Table 2 to create plausible futures. Note that multiplier ranges in this Table represent plausible rather than probable values. They provide a mechanism for understanding how wrong our baseline model assumptions can be before significant vulnerabilities to deep uncertainties occur (Herman et al., 2014). The 4 economic multipliers in this analysis are interest (discount) rate, $r$, cost overruns, $C_{or}$, during construction, and two energy prices, reflecting Turkey's energy regulations; $p_{1-10}$ is fixed for the first 10 year by the Turkish government, including subsidies and $p_{>10}$ is the energy price for the remainder of the project's lifetime. The 3 hydroclimatic multipliers are streamflow statistics: its median, coefficient of variation and first percentile. A comprehensive justification for all these parameters and their associated sampling ranges can be found in the supporting information for Yildiz et al. (2024).

Once the variable ranges are set, we generate a 7-dimensional Latin Hypercube Sample of 500 plausible futures to represent the deep uncertainties across socio-economic and hydroclimatic futures. Note that we use the three hydroclimatic parameters to parameterize a unique FDC for each plausible climate future (Yildiz et al., 2023).

## 3. HYPER-FORD

We now move to the middle gray box of Fig. 1, where we introduce the HYPER-FORD approach and its two innovations for robust and computationally efficient optimal design. In Section 3.1, we first introduce the optimization module, HYPER$_{OP}$, tailored for joint design and operation optimization. Subsequently, in Section 3.2, we present the FDC approximation module build upon HYPER$_{OP}$ aimed at enhancing computational efficiency through regular sampling of the FDC.

### 3.1. Coupled design and operation optimization: HYPER$_{OP}$ module

In the earlier versions of the HYPER toolbox (Yildiz and Vrugt, 2019; Yildiz et al., 2024), the distribution of available inflow between the different turbines was regulated by operational rules that reflect engineering practice. According to these rules, and outside of the extreme cases where turbines shut down in instances of very small or excessively large river discharge, water is allocated to the maximum number of turbines at full capacity, with any remaining flow directed to other turbines capable of operation. This approach does not explore alternative operational modes that could result in higher power production. For instance, two turbines operating efficiently at 75% capacity may generate more power than one turbine at full capacity and another at a lower capacity, as the latter may result in reduced efficiency or even shutdowns due to technical constraints.

To address these issues, this study presents a new version of HYPER, called HYPER$_{OP}$ – where 'OP' stands for the first two letters of

**Table 1**
Hydrological and site characteristics of the RoR hydropower plant case studies.

| Case Study | Mean [$m^3/s$] | Coefficient of Variation [-] | Environmental flow [$m^3/s$] | Gross Head [m] | Potential GAAE [GWh] |
|---|---|---|---|---|---|
| Besik | 5.8 | 0.59 | 0.63 | 117 | 58.31 |
| Buyukdere | 1.88 | 1.09 | 0.156 | 394 | 63.65 |
| Tepe | 6.22 | 1.39 | 0.662 | 56 | 29.93 |
| Karacay | 1.47 | 1.69 | 0.18 | 134 | 16.92 |
| Kaplan | 1.07 | 1.08 | 0.12 | 190 | 17.47 |

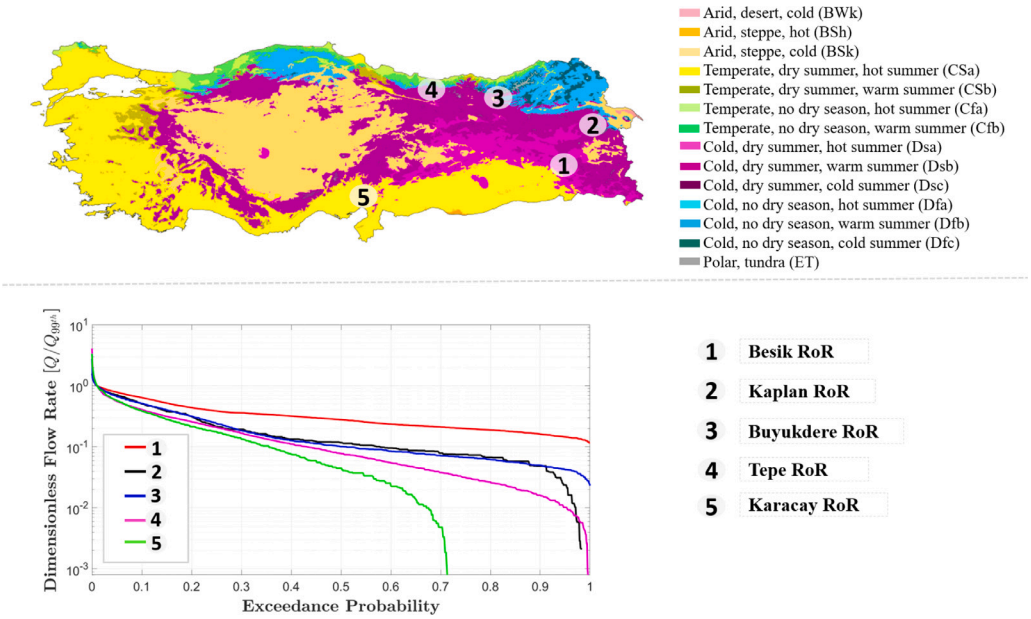


**Fig. 3.** The top panel displays the geographical locations of the five case studies on the Köppen–Geiger climate classification map of Turkey (Beck et al., 2018). In the bottom panel, Flow Duration Curves (FDC) for these case studies are shown, with normalization applied using the 99th percentile of the flow. The flow rate values on the *y*-axis are presented logarithmically.

**Table 2**
Variables and sampling ranges used for robustness analysis. SF is for scaling factor, and a SF of 1 indicates baseline conditions. The initial four are economic parameters, while the three hydroclimatic parameters (highlighted in blue) pertain to streamflow statistics used in the construction of future streamflow time series.

| Uncertain Factor | Current Value | Lower Bound | Upper Bound |
|---|---|---|---|
| Interest (discount) rate ($r$) | 0.095 | 0.03 | 0.15 |
| Energy price, first 10 years ($p_{1-10}$) | 5.5 | 5 | 6.5 |
| Energy price, rest of the years ($p_{>10}$) | 5.5 | 3 | 6.5 |
| Cost overrun ($C_{or}$) SF | 1 | 1 | 3 |
| Median SF ($\tilde{m}$) SF | 1 | 0.3 | 1 |
| Coefficient of Variation ($CV$) SF | 1 | 1 | 2 |
| 1st percentile ($P_{1st}$) SF | 1 | 0.3 | 1 |

both words in "operation optimization". HYPER$_{OP}$ integrates optimized turbine operations into the design process, optimizing the allocation of flow to turbines during the simulation phase. This optimization ensures that the allocation of turbine flow is aligned with their unique characteristics, thereby enhancing overall efficiency. The operation optimization module (OP module), nested within the optimization algorithm, is presented in Algorithm 1 as pseudo-code. For each set of design parameters generated by the optimization algorithm, the OP module initially defines the operating range within which turbines can generate energy (minimum flow and maximum flow). It then divides this range into $I = 1000$ discrete steps. For each step, the OP module generates $J = 1000$ random samples of turbine numbers and their corresponding operation capacities to simulate energy generation. We propose $I = 1000$ and $J = 1000$ as our testing indicated it was enough to reliably provide operation optimization for designs up to 3 turbines, the maximal number of turbines considered for small (< 10MW) RoR hydropower plant design. Following this process, the OP module records the optimal settings derived from these samples, thereby constructing a table of operation modes for use in subsequent simulation optimization. In cases where there are less than 1000 flows considered in the operational range of the plant, such as in FDC discretization detailed in Section 3.2, the OP module relies solely on these flows to determine operation modes. This study represents the first instance of coupled design and operation optimization for RoR hydropower plants without any limitations on turbine configuration for up to three turbines. By contrast, traditional configurations involve identical turbine, or in three-turbine setups, one small and two large turbines.

Fig. 4 showcases the optimized operating modes of a triple Francis turbine configuration, having one small turbine ($T_1$, with a design discharge of 5 $m^3/s$) and two large turbines ($T_2$, each with a design discharge of 10 $m^3/s$). The operational range (top panel) is finely divided into 1000 increments spanning from the minimum flow rate of 2 $m^3/s$ (equivalent to 40% of $T_1$'s design discharge) to the maximum flow rate (design discharge) of 25 $m^3/s$. In the bottom panel,

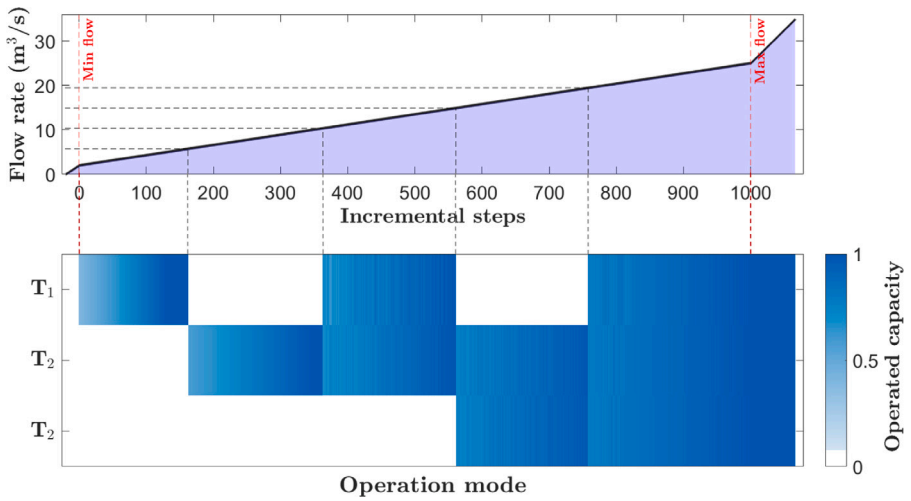


**Fig. 4.** Top panel: The operational range of a triple Francis turbine setup featuring one small turbine ($T_1$, design discharge: 5 $m^3/s$) and two large turbines ($T_2$, 10 $m^3/s$ each). The range is discretized into 1000 increments between the minimum (2 $m^3/s$, corresponding to 40% of $T_1$'s design discharge) and maximum (25 $m^3/s$) flow rates. Vertical black dashed lines delineate transitions between turbine operating modes. Bottom panel: Representation of the respective operational modes of the turbine(s) with their operated flows depicted based on the incremental steps outlined in the top panel. The color bar indicates turbine operation capacity, with white representing no operation and darker blue indicating higher capacity.

**Algorithm 1:** Pseudocode for operation optimization algorithm

**input :** Turbine configuration parameters: type, number, capacities
**output:** Table of operation modes for each configuration

```
for Each sampled turbine configuration: type, number, capacity do
    Determine each turbine's flow range: min flow and max flow;
    Divide the flow range into I = 1000 discrete steps;
    for i = 1, ..., T do
        Draw J = 1000 random samples of turbine numbers and their operation capacities;
        for j = 1, ..., J do
            Simulate energy generation;
        Determine and record the sample j* that maximizes energy generation;
    Create a table of operation modes for the current turbine configuration;
```

the operational modes of the turbines and their respective operating capacity are provided based on the incremental steps outlined in the top panel. Notably, turbines are programmed to shut down when the flow rate falls below their technical minimum flow rate. Subsequently, only the small turbine operates until the flow rate reaches a level efficient for the activation of the second and third turbines. All three turbines operate at full capacity when the flow rate surpasses the design discharge. This visualization offers comprehensive insights into the optimized operational dynamics of the turbine system across varying flow conditions.

### 3.2. Flow duration curve discretization: approximation module

A multi-year daily FDC can be approximated by a small number of values, regularly spaced on the $x$-axis. Fig. 5 illustrates this, and features 27 years of the daily flows for the Besik case study, resulting in 9860 daily discharge values. It also shows a sampling using $N = 50$ discharge values (depicted as black dots). It is evident that this regular sampling, in lieu of several decades of daily flows significantly reduces the computational costs associated to the performance evaluation of each design, both during simulation optimization and during robustness analysis. This is particularly notable since each flow value is repeatedly used in each iteration: for calculating hydraulic losses, for water allocation to the turbines, to evaluate the efficiency of the turbines, and to determine energy generation.

In the optimization process, we sample $N$ evenly distributed points from the historical time series (black dots on Fig. 5). Likewise, we apply this discretization to each of the 50 time series used to evaluate each plausible future during the subsequent robustness analysis. For both of these approximation steps, at each sampled point $n$ ($1 \leq n \leq N$), we rely on the optimized operations provided by $\text{HYPER}_{OP}$ to yield the flow rate $q_k(n)$ at each turbine $k$ of the $K$-turbine hydropower plant ($K \in \{1, 2, 3\}$). Then, the average annual power generation $AAE$ that a $K$-turbine hydropower plant ($K \in \{1, 2, 3\}$) can produce over a year is given by:

$$AAE = Y_{\text{hr}}\ \rho\ g \sum_{n=1}^{N} \sum_{k=1}^{K} \eta_k(q_k(n))\ q_k(n)\ H_{\text{net}}(q_k(n)) \tag{9}$$

where $Y_{\text{hr}}$ is the number of hours in 365 days, $\rho$ is the volumetric mass density of water, $g$ is the gravitational acceleration constant, $H_{\text{net}}$ is the hydraulic head, and $\eta_j$ is turbine efficiency. Note that both $H_{\text{net}}$ and $\eta_j$ are time dependent and vary as function of turbine inflow, penstock diameter and/or design flow, respectively. We can then approximate the annual plant revenue as follows:

$$\text{Revenue in year } y,\ R_y = AAE * p_y \tag{10}$$

where $p_y$ is the energy price during year $y$. This time dependence of energy price enables to incorporate regulatory price incentives, among other considerations. Computation of this revenue approximation enables that of both financial objectives (NPV and BC) and robustness metrics ($RM_{\text{PB}}$ and $RM_{\text{NPV}}$).

## 4. Benchmarking the modifications to HYPER-MORDM

In this section, we describe the benchmarking experiments outlined in the bottom gray box of Fig. 1. First, Section 4.1 details the methodology applied to benchmark of $\text{HYPER}_{OP}$. Sections Section 4.2, 4.3, and 4.4 explain the benchmarking methodology for using an approximation of the FDC, respectively in the optimization step, the robustness analysis step and when integrating both steps in a unified workflow. Table 3 provides a summary of the benchmarking process

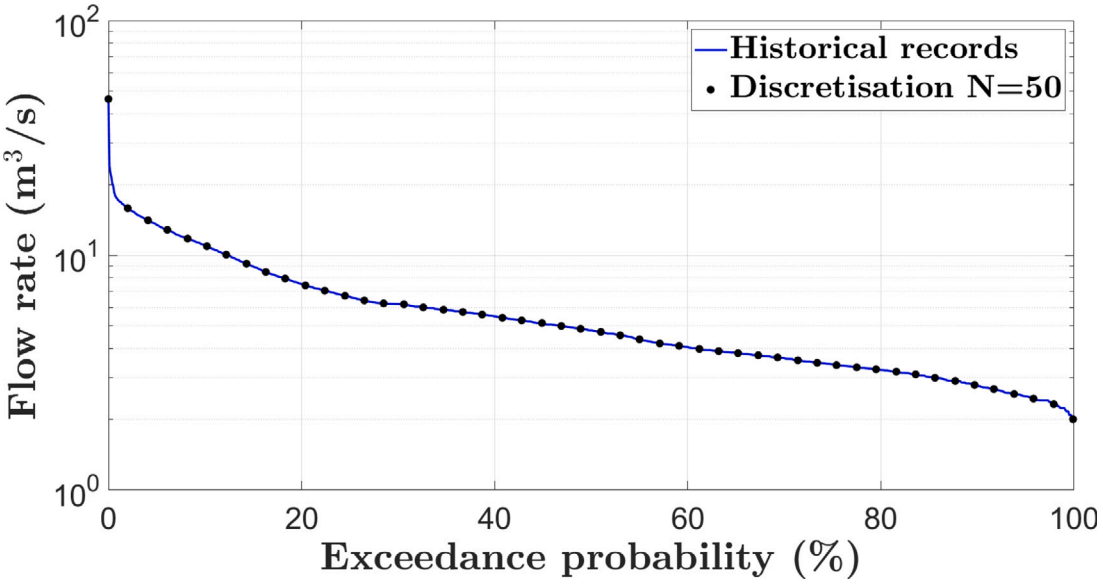


**Fig. 5.** Plot of the flow duration curves (FDC) of 27 years daily discharge record comprising 9860 data points (blue line) and $N = 50$ sampled flow rates (black dots).

**Table 3**
Benchmarking experiments of each step.

| Benchmarking Step | Methodologies Applied | Case Study Used |
|---|---|---|
| 4.1 $HYPER_{OP}$ | – Comparison of Pareto sets generated by HYPER and $HYPER_{OP}$ through two-objective optimization.<br>– Comparative analysis of energy generation from the two models for the same design alternatives. | Besik RoR |
| 4.2 FDC approximation during multi objective optimization | Evaluation of Pareto sets generated by $HYPER_{OP}$ using FDC approximation and long-term records, assessed with key metrics including hypervolume, generational distance, $\epsilon$–indicator, and runtime. | Besik RoR |
| 4.3 FDC approximation during robustness analysis | Assessing the robustness of design alternatives from FDC approximation versus long-term records by comparing their relative ranking and runtime. | Besik RoR |
| 4.4 FDC approximation across the whole analysis | In-depth comparison of alternatives generated through coupled design optimization and robustness analysis, using FDC approximation and long-term records. | All of the five cases |

at each step. The first three benchmarking steps only use the Besik RoR hydropower plant, as this is a typical candidate location for such a plant: this case study is anticipated to be the most profitable according to traditional assessments of RoR plants. The other four sites are used as an additional check on the quality of the full workflow of the HYPER-FORD in Section 4.4. Both design optimization and robustness analysis are performed using MATLAB on a computer equipped with an Intel(R) Core(TM) i7-10700 CPU operating at 2.9 GHz, supported by 16 GB RAM, and running the Windows 10 operating system. The analytical outcomes of all four benchmarking processes will then be presented in Section 5.

### 4.1. Benchmarking of $HYPER_{OP}$

The benchmarking of $HYPER_{OP}$ – joint optimization of design and operations – aims at comparing it with the original HYPER toolbox. In order to obtain the Pareto optimal set of alternatives, both HYPER and $HYPER_{OP}$ are integrated into a simulation–optimization setup with the Amalgam MOEA introduced by Vrugt and Robinson (2007) – the performance of this MOEA was benchmarked in Yildiz et al. (2024). All MOEA searches throughout this paper are conducted using a population size of $I = 100$ individuals and running Amalgam for $J = 1000$ generation, with an explicit two objective formulation (Eq. (5)). We chose the two-objective formulation of Eq. (5) to benchmark the new innovation, in order to provide a thorough analysis of $HYPER_{OP}$ increases solution quality of diverse solutions along the Pareto front.

In this benchmarking process, we assess $HYPER_{OP}$ in two distinct ways. Initially, for the problem, we carry out a HYPER optimization and a $HYPER_{OP}$ optimization to generate two distinct Pareto sets of alternatives. By comparing these Pareto sets, we aim to discern differences in the objective values of the alternatives, evaluating the $HYPER_{OP}$'s ability to produce designs with improved objective values and novel solutions. Subsequently, we take the set of design alternatives proposed by the original HYPER toolbox, and use them in $HYPER_{OP}$ in simulation mode to quantify how optimized operations increase the energy generation of each alternative. This step allows us to verify that $HYPER_{OP}$ functions as intended.

### 4.2. Benchmarking of FDC approximation during multi objective optimization

To benchmark multi objective optimization through the FDC approximation, we explore alternative designs (Pareto sets) generated

using the HYPER$_{OP}$, still focusing on the Besik RoR hydropower plant. Initially, we generate a reference Pareto set with the long-term discharge record. Subsequently, we generate Pareto sets based on regular samplings of this discharge record, with sample sizes $N = 10, 25, 50, 100, 200,$ and $500$. During optimization, the performance of solutions is evaluated using Eqs. (9) and (10), with consideration given to the approximated revenue.

Our analysis assesses the performance of FDC approximations by using classic key performance measures (Reed et al., 2013; Salazar et al., 2016): hypervolume, generational distance, additive $\epsilon-$indicator, and run time. Hypervolume quantifies the volume of the objective space that is dominated by the provided set of solutions with respect to a reference point, ensuring this measure combines proximity and diversity (Hadka and Reed, 2012). Hypervolume computation requires defining an easily interpretable 0–1 scale, with 0 defined by an appropriate origin point. In our analysis, we begin by normalizing the objective functions and by placing the origin point as being 10% worse than the worst value of each objective in the reference Pareto set (Ishibuchi et al., 2018), computed with the long-term discharge record. We consider the hypervolume of the reference Pareto set as 1. These choices enable a rigorous quantification of how far results using the FDC approximation are from those using the actual flow record. Hypervolume is complemented by generational distance (Van Veldhuizen, 1999), which calculates the average Euclidean distance between the solutions of the approximation set and the nearest member of the reference set. This metric primarily assesses convergence, yet it does not offer information regarding the diversity of the solution set (Blank and Deb, 2020). The additive $\epsilon-$indicator (Zitzler et al., 2003) evaluates the maximum distance needed to move an approximation set solution in order to dominate its nearest neighbor in the reference set. This metric is particularly sensitive to the presence of gaps and the overall diversity within the approximation set rather than convergence (Reed et al., 2013).

We also examine the optimization runtime for the long term record and each sample size, aiming to understand the relationship between sample size and run time, key to finding a good compromise between computational gains and solution quality.

Additionally, we further our analysis using an alternative metric, defined as the count of efficient solutions within the Pareto set. Alternatives generated from each FDC approximation are reevaluated with the long-term record to reveal their "true" objective values. Some solutions in the resulting set may be dominated – in the Pareto sense – by others. Our new metric evaluates the ability of approximations to generate solutions that would still be Pareto efficient with the full historical data at our disposal. These metrics, taken together, are intended to provide a comprehensive assessment of solution quality and trade-offs in our analysis, between improving run time and improving solution quality.

### 4.3. Benchmarking of FDC approximation during robustness analysis

Continuing from the previous section, we employ the Besik RoR to evaluate the effectiveness of the introduced sampling methodology in approximating robustness. For this, we compare robustness evaluations for solutions given by HYPER$_{OP}$ and obtained with the full historical record. We proceed to evaluate the robustness of these same alternatives using the same sample of plausible futures. For each sampled future, we replace the 50 synthetically generated multi-decadal daily time series with sampling of these time-series with varying sample sizes $N = 10, 25, 50, 100, 200,$ and$; 500$. Similar to what happens in the optimization step, the methodology described in Section 3.2 is used to approximate hydropower production in benefits for each sampled FDC.

Compared with long-term future flow FDCs, we investigate the extent to which the relative ranking of alternatives based on their robustness is affected by FDC sampling . Said otherwise, we are examining whether an alternative that initially ranks high (or low) in robustness based on long-term future flows maintains that ranking when robustness is computed based on a small number of sampled point for each plausible future FDC. We specifically focus on alternatives having the highest objective values, such as the best NPV and best BC, as well as the most robust alternative. Additionally, we evaluate the runtime for each sample size to gain insights into how computational efficiency correlates with sample size and the quality of robustness results. Ultimately, our goal is to determine the sample size that offers a sufficiently accurate approximation of long-term futures in terms of robustness. This analysis is performed separately for the two defined robustness metrics.

### 4.4. Benchmarking of FDC approximation across the whole analysis

After benchmarking the impact of FDC approximations on optimization and robustness separately, we now aim at assessing the combined impact across the full workflow, both on run time and solution performance. We focus on how similar or different the design recommendations are, depending on whether we use the full historical record or a regularly spaced sample of it. For this, we use all five case studies presented in Section 2.3 to ensure that the approximation maintains performance across a range of site and climate characteristics. Initially, we generate design alternatives using the HYPER$_{OP}$ module with long-term discharge records, with the same optimization setup as in Section 4.2. Subsequently, we assess their robustness across our sample of 500 plausible futures. Next, we generate design alternatives using the same experimental setup, but with the sample size of discharge records set to a value of $N$. We choose that value based on benchmarking results for the use of FDC approximations in both optimization and robustness analysis steps. Following this, we quantify the robustness of alternatives across the sampled futures.

By comparing design alternatives and their robustness from long-term futures flows with those derived from selected sampled points, we aim to evaluate whether the overall approximated methodology produces similar robust designs. Our analysis of the design parameters specifically focus on key alternatives such as the most robust alternative, and alternatives with the highest NPV or BC value.

## 5. Results

In this section, we present results for the benchmarking exercises in the same order as they are presented in Section 4. We initially investigate the performance analysis and validation of optimization module, HYPER$_{OP}$ (Section 5.1). Our focus then shifts to HYPER$_{OP}$ with the FDC approximation analysis within the context of multiobjective optimization (Section 5.2), robustness (Section 5.3), and both steps combined (Section 5.4). Note that the computational experiments were conducted under the same conditions during both optimization and robustness analysis, with the only difference being the size of the input data (e.g., in Figs. 9 and 10 and Tables 6 and 7).

### 5.1. HYPER$_{OP}$ validation and performance

The performance analysis of the HYPER$_{OP}$ is depicted in Fig. 6, with a comparison with the HYPER toolbox across the NPV (x-axis) and BC (y-axis) objective space. The design alternatives generated by optimization with HYPER (white dots) and HYPER$_{OP}$ (red dots) are compared in the panel A. Thanks to inbuilt operation optimization, HYPER$_{OP}$ clearly yields a diverse Pareto optimal set with higher objective values, offering a selection of design alternatives that effectively balance multiple objectives. There is a gap in the Pareto front of design alternatives generated through the HYPER toolbox, while no such gap exists in the Pareto front of design alternatives generated through HYPER$_{OP}$. This happens because HYPER solely depends on fixed operating conditions (rule curves), introducing technical thresholds that lead to discontinuities in the relationship between flows through the turbine and power output, leading in turn to discontinuities

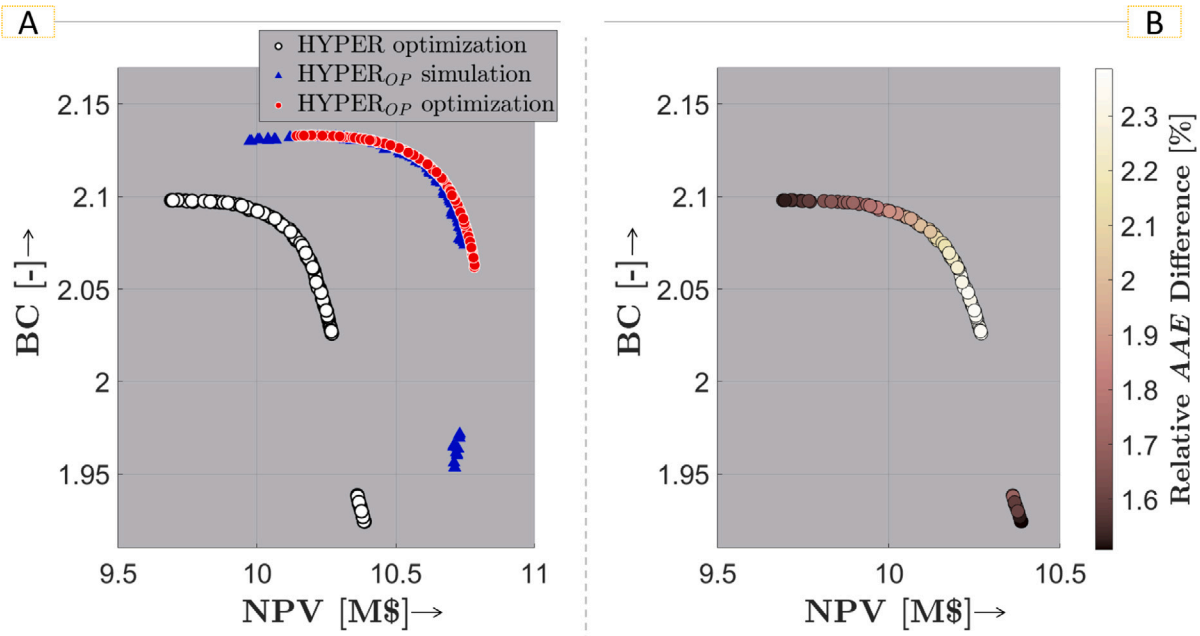


**Fig. 6.** Panel A: Pareto sets derived by HYPER (white dots) and HYPER$_{OP}$ (red dots) on the two-dimensional Benefit–Cost Ratio (BC) and Net Present Value (NPV, in million dollars) objective space. Blue triangles indicate HYPER solutions within the context of HYPER$_{OP}$. Panel B: Performance comparison of HYPER and HYPER$_{OP}$ for the same Pareto solution set. The color bar illustrates the relative annual average energy (AAE) difference between the two, with light colors indicating higher relative differences (HYPER$_{OP}$ outperforming HYPER). Arrows on the plot labels indicate the direction of preference.

in the Pareto front. These discontinuities disappear with the built-in optimization that characterizes HYPER$_{OP}$. This robust performance underscores its efficient optimization capability.

Upon reevaluating HYPER alternatives (white dots in panel A) using HYPER$_{OP}$ in simulation mode, we observe an increase in the objective values for all alternatives, as denoted by the blue triangles. Note that some of the blue triangles are dominated after reevaluation. We also observe a close correlation between optimal solutions yielded by HYPER$_{OP}$, and HYPER solutions reevaluated with HYPER$_{OP}$. This suggests that the improvement in objective values brought about by HYPER$_{OP}$ is mostly due to the operation optimization, and the increase in energy generation this leads to. Panel B, which presents a comparison of energy generation performance between the two models for the same Pareto solution set (white dots in panel A), quantifies this increase. There is an approximate 2% increase in energy generation for all the alternatives. Together with the findings from the left panel, these results indicate that HYPER$_{OP}$ outperforms HYPER, primarily because it optimizes the operation that better captures streamflow variability instead of relying on operational rules for energy generation. This being said, the magnitude of the improvement is small, underscoring why operation optimization has been a low priority in design procedures in the past.

### 5.2. FDC sampling impact on multi-objective optimization

In this section, we compare the results obtained from analyzing the design alternatives generated through FDC approximation with those derived from long-term records for the Besik case study.

Table 4 provides a comparison of various performance metrics for optimization results using long-term records, vs. optimization results using $N$ sample points, for different values of $N$. Notably, the computational time required for generating alternatives is over 3.6 h when using long-term records, whereas it is under 11 min for a sample sizes of $N = 100$ points, a factor of 20. The runtime's scaling with sample size is not linear, primarily due to the algorithm used for operation optimization (see Algorithm 1). Indeed, for long-term records, the OP module handles optimization tasks for a maximum of 1000 incremental flow rates, which somewhat limits gains from sampling. When sampling the FDC, the OP module only uses sampled points of the FDC that are within the flow range, which means that it handles only a subset of the $N$ sampled points, resulting in non-linear scaling. Still in Table 4, the hypervolume performance for sample sizes of $N >= 50$ points is in close proximity to the Reference Pareto Front (RPF), indicating that the solution set exhibits both convergence and diversity. Note that the RPF was generated from 5 trials with different random seeds. The generational distance for sample sizes of $N >= 100$ points closely approach the values from the RPF. This indicates that the solutions have converged effectively, demonstrating the overall quality of the obtained solution set. Likewise, the $\epsilon$–Indicator for sample sizes of $N > 50$ points closely aligns with the RPF values, signifying the overall diversity within the approximation set is robust. As the sample size decreases below $N = 100$, the proportion of efficient solutions also decreases. In comparison, when $N >= 50$ points are considered, a substantial 80% of the solutions fall within the Pareto set.

Fig. 7 provides a comparison between design alternatives obtained from $N = 10$ sampled points (blue dots, left panel) and $N = 100$ sampled points (red dots, right panel) with design alternatives derived from the RPF. The alternatives generated from sampled points (blue dots and red dots) are subsequently reevaluated using the long-term record to unveil their "true" objective values. Alternatives marked with triangles represent Pareto frontiers on both panels, indicating that these solutions dominate all other points within the set. It is evident that with a smaller sample size ($N = 10$), a large amount of solutions deviate from the RPF. However, for $N = 100$, it is clear that the re-evaluated Pareto front is very close to the RPF, and what is more, it comprises most design alternatives. This coincides with the metrics from Table 4, and illustrates the accuracy and reliability of optimization outcomes when regularly sampling $N = 100$ FDC points.

### 5.3. FDC sampling impact on robustness analysis

In this section, we provide a detailed examination of the robustness of the design alternatives forming the RPF used in the previous section, and the impact of FDC approximation on robustness results. In Fig. 8, the parallel plot showcases various design alternatives. The top panel represents robustness metric $RM_{\mathrm{PB}}$, while the bottom panel showcases

**Table 4**
Performance metrics for multi-objective optimization of long term discharge data and of different sample sizes ($N$ = 10, 25, 50, 100, 200, and 500).

| Number of Points | Optimization Run Time (minutes) | Hypervolume | Generational Distance | Additive $\epsilon$−Indicator | Percentage of Efficient Solutions [0-100] |
|---|---|---|---|---|---|
| 10 | 1.37 | 0.94 | 8.84 $10^{-4}$ | 0.0064 | 53 |
| 25 | 3.05 | 0.97 | 5.07 $10^{-4}$ | 0.0053 | 72 |
| 50 | 5.24 | 0.98 | 3.34 $10^{-4}$ | 0.0104 | 77 |
| 100 | 10.28 | 0.98 | 9.41 $10^{-5}$ | 0.0032 | 85 |
| 200 | 31.72 | 0.98 | 9.95 $10^{-5}$ | 0.0.031 | 83 |
| 500 | 82.53 | 0.99 | 9.86 $10^{-5}$ | 0.0021 | 90 |
| Long Term | 216.96 | 1 | 0 | 0 | 100 |

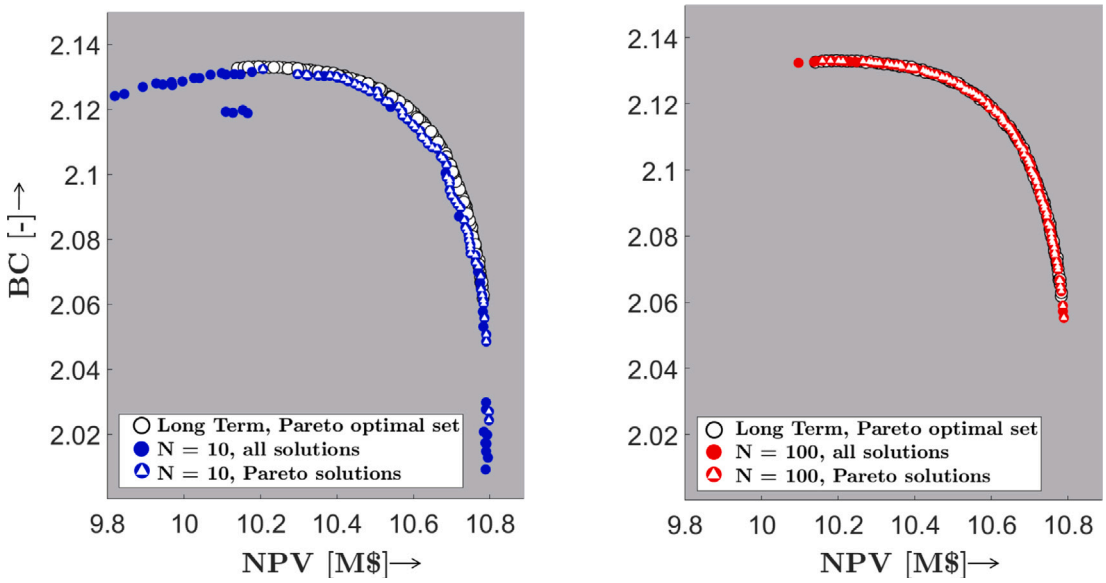


**Fig. 7.** Performance comparison of the reference Pareto front (RPF) obtained with optimization using the long-term FDC, with solutions obtained with optimization using the sampled FDC, and whose performance is re-evaluated using the long-term record. For $N$ = 10 (left panel) and $N$ = 100 sampled points (right panel), solutions that are non-dominated in the re-evaluated set are figured with white triangles. Arrows on the plot labels indicate the direction of preference.

$RM_{\mathrm{NPV}}$, and both plots are organized in the exact same way. Each line represents one alternative and presents (i) the values of the $f_{\mathrm{BC}}$ and $f_{\mathrm{NPV}}$ design objectives, as well as (ii) the two financial robustness measures based on the dataset size (long term and sampled size). The robustness measures along the vertical axis at the "Long Term" section serve as reference values since they are derived from long-term records, and compared with the robustness of the same design evaluated using different FDC approximations. The color of each line in both panels corresponds to its BC value, with yellow indicating a high BC and magenta indicating a low BC. This Figure also emphasizes the alternative with the highest NPV value (red line), the alternative with the highest BC value (green line), and the most robust alternative as identified with approximation-free robustness evaluation (black line). Clearly, there is a noticeable positive correlation between both robustness metrics and $f_{\mathrm{BC}}$, and a negative correlation with $f_{\mathrm{NPV}}$. This is because alternatives with higher $f_{\mathrm{BC}}$ values tend to be smaller in design, resulting in lower costs, making them better suited for a drought-prone world (Yildiz et al., 2024).

This setup enables exploring the impact of FDC approximations and sample size $N$. Even though the robustness metric values are slightly higher for the sampled points in both panels, the overall pattern of the reference robustness metric values closely resembles that of the sampled points. This indicates that the ranking of robust solutions remains largely consistent. For example, in both panels, the best NPV alternative exhibits the lowest robustness metric with long term record, a trend that holds true for the sampled points as well. The MR alternative, identified based on long-term flows, consistently emerges as one of the most robust solutions for $RM_{\mathrm{NPV}}$ across all sample sizes, and for $RM_{\mathrm{PB}}$ when the sample size $N >= 25$. Likewise, the best BC alternative demonstrates a similar robustness metric to the MR alternative in both panels, a consistency observed across different sampling sizes. However, notable deviations occur in the results for $RM_{\mathrm{PB}}$ when the sample size is small, $N <= 50$. This is where lines begin to intersect, and the differences between solutions get smaller, indicating a loss of reliability of the robustness metric. Similarly, there is a substantial divergence in the results for $RM_{\mathrm{NPV}}$ when the sample size $N < 50$.

The computational time for robustness analysis across various sample sizes is summarized in Fig. 9. Significantly, the runtime exceeds 26 h when utilizing long-term records, while it remains under 2 h for sample sizes of $N \leq 100$ points, representing a reduction factor of 15. For more detailed information on run time, please refer to Table 6 in the appendix. These results, when taken together, suggest that sampling futures with $N >= 50$ for robustness analysis provides a reliable and efficient approximation. Therefore, to align with the optimization analysis results, we selected $N = 100$ to conduct the robustness analysis with other case studies as discussed in the next section.

### 5.4. Whole-workflow impact of FDC sampling

In this section, we present the outcomes of our analysis across all study sites listed in Section 2.3. Our primary focus lies in comparing the coupled optimization and robustness analysis as well as runtime for three selected alternatives: the solution with the best NPV, the solution with the best BC, as well as the solution with the highest $RM_{PB}$ value, identified as the Most Robust (MR).

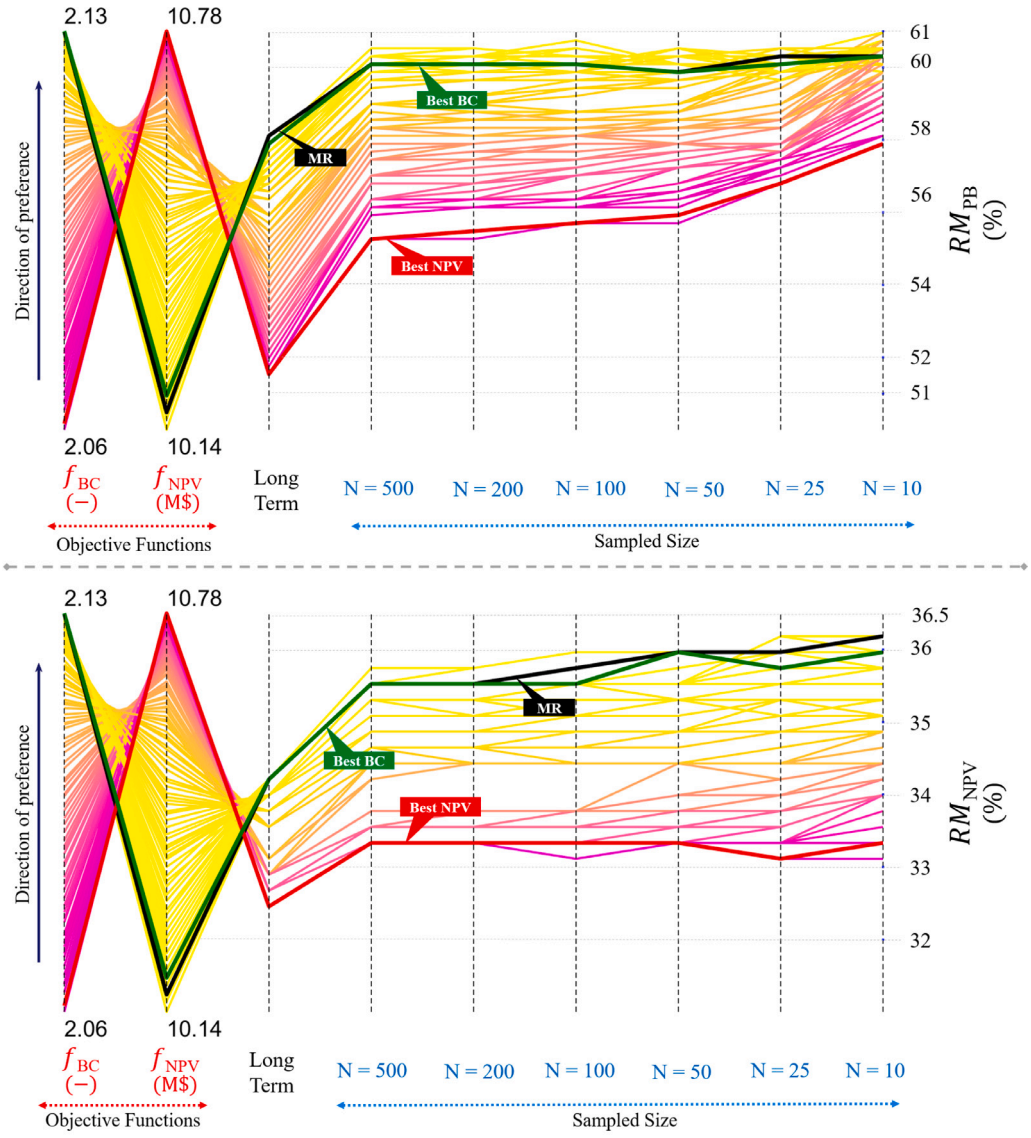


**Fig. 8.** The parallel plot of two objective functions: $f_{BC}$ (-), $f_{NPV}$ (M$), along with their respective robustness measures, for different sample sizes ($N$ = 10, 25, 50, 100, 200, and 500). In the top panel, the robustness measure is represented by $RM_{PB}$, while in the bottom panel, it is denoted as $RM_{NPV}$. Color coding on the lines is utilized to classify the results based on the value of $f_{BC}$.

Table 5 presents the design characteristics, financial and energy performance metrics, and robustness metrics for these selected alternatives of each case. The data is displayed for two scenarios: long-term records (white background) and based on a sample size of $N$ = 100 (gray background). It is evident that while the financial and robustness metrics of Best NPV and Best BC obtained through long-term discharge record and $N$ = 100 sampled points are slightly different from each other, their design characteristics including turbine type, number and their respective capacities remain remarkably consistent across all the cases, regardless of FDC sampling. While sampling only $N$ = 100 discharge values may lead to some loss of discharge information that affects these financial metrics, the impact on their design optimization is relatively minimal. This underscores the robustness of the approach across different scenarios, highlighting its reliability in diverse cases.

Notably, in each case-study the MR alternatives derived using FDC sampling exhibit similar design characteristics as those derived using long-term data — including turbine configuration and their respective capacities. An exception is observed in the Tepe case, where the most robust alternative features a different turbine setup. However, another robust alternative, with very similar robustness metric score, closely mirrors the design parameters observed in the long term record. This is particularly significant since these alternatives are selected through robustness analysis. The fact that sampling the future scenarios considerably decreases computational costs and resources while still yielding similar MR alternatives shows the consistency and dependability of the proposed approach in assessing the robustness of RoR designs. It is also interesting to note that the Tepe RoR case's optimal NPV alternatives on both scenarios include a triple turbine configuration consisting of two small and one large turbine. Traditionally, three-turbine systems for RoR hydropower plants employ one small and two large (identical turbines). The novel turbine operation optimization module included in HYPER$_{OP}$ model has led to the identification of this new alternative with higher performance metrics. This demonstrates the capability of HYPER$_{OP}$ to explore optimal solutions beyond conventional engineering norms.

The runtime for optimization, involving 20–30 years of daily discharge data with 100,000 function evaluations is substantially reduced by over 91% for $N$ = 100 sampled points and by over 97% for $N$ = 50 sampled points in each case study as shown in top panel of Fig. 10. Likewise, the runtime for robustness analysis (as shown in the bottom panel of Fig. 10) across 500 plausible scenarios shows a significant decrease of over 92% for $N$ = 100 sampled points and over 93% for $N$ =

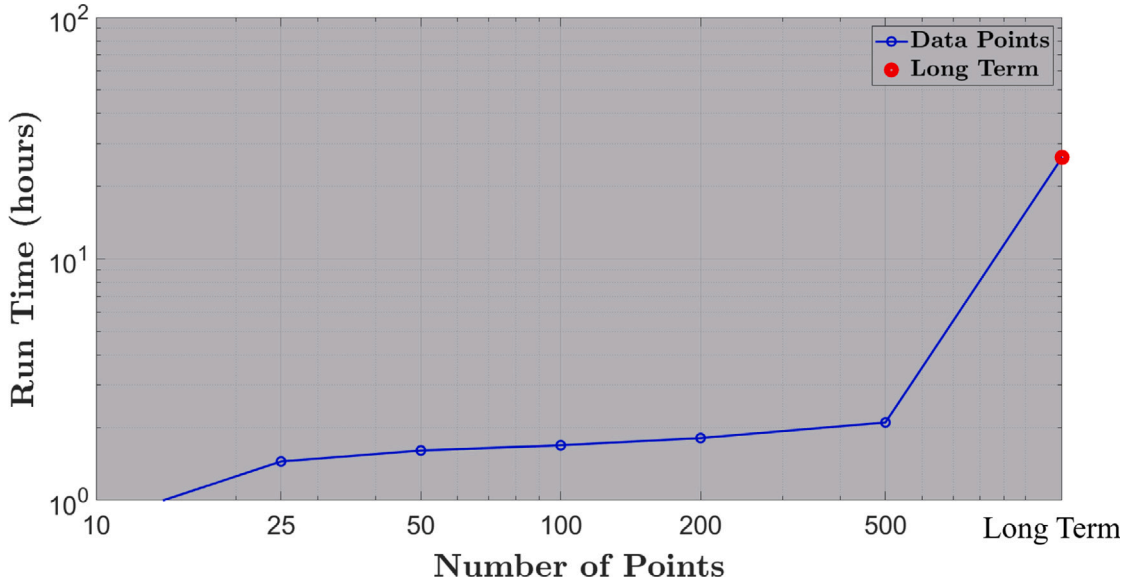


**Fig. 9.** Robustness analysis run times for long term discharge data and of different sample sizes ($N$ = 10, 25, 50, 100, 200, and 500). The $y$-axis is on a logarithmic scale.

**Table 5**
Design characteristics, performance metrics and robustness of the most robust (MR) alternative and the alternative with highest NPV and BC of given five case studies.

| Case Study | Methodology Alternatives | Turbine Configuration | Design Discharge [$m^3/s$] | $IC$ [MW] | $AAE$ [GWh] | $f_{NPV}$ [M$] | $f_{BC}$ [-] | $RM_{PB}$ [%] | $RM_{NPV}$ [%] |
|---|---|---|---|---|---|---|---|---|---|
| Besik | Long Term, **MR** | Dual Francis | 2.00–3.27 | 5.99 | 34.13 | 10.17 | 2.13 | 58.11 | 34.21 |
| Besik | Long Term, **BC** | Dual Francis | 2.03–3.28 | 6.03 | 34.22 | 10.19 | 2.13 | 57.80 | 34.21 |
| Besik | Long Term, **NPV** | Dual Francis | 2.70–3.98 | 7.60 | 37.34 | 10.78 | 2.06 | 51.53 | 32.45 |
| Besik | $N$ = 100, **MR** | Dual Francis | 2.10–3.40 | 6.26 | 34.83 | 10.36 | 2.13 | 60.74 | 35.53 |
| Besik | $N$ = 100, **BC** | Dual Francis | 2.03–3.28 | 6.03 | 34.22 | 10.19 | 2.13 | 60.08 | 35.53 |
| Besik | $N$ = 100, **NPV** | Dual Francis | 2.70–3.97 | 7.60 | 37.33 | 10.78 | 2.06 | 55.70 | 33.11 |
| Buyukdere | Long Term, **MR** | Dual Pelton | 0.72–1.50 | 7.41 | 29.68 | 8.41 | 2.02 | 65.8 | 39.4 |
| Buyukdere | Long Term, **BC** | Dual Pelton | 0.54–0.96 | 4.85 | 23.68 | 6.97 | 2.10 | 60.6 | 37.8 |
| Buyukdere | Long Term, **NPV** | Dual Pelton | 0.91–1.96 | 9.84 | 34.15 | 8.94 | 1.88 | 63.0 | 37.0 |
| Buyukdere | $N$ = 100, **MR** | Dual Pelton | 0.75–1.63 | 7.99 | 30.81 | 8.60 | 1.99 | 68.2 | 39.8 |
| Buyukdere | $N$ = 100, **BC** | Dual Pelton | 0.54–0.98 | 4.94 | 23.95 | 7.05 | 2.10 | 63.6 | 38.4 |
| Buyukdere | $N$ = 100, **NPV** | Dual Pelton | 0.93–2.06 | 10.24 | 34.78 | 8.97 | 1.85 | 66 | 38 |
| Tepe | Long Term, **MR** | Dual Francis | 1.84–4.63 | 3.54 | 14.05 | 2.94 | 1.59 | 54.0 | 28.0 |
| Tepe | Long Term, **BC** | Dual Francis | 1.46–3.46 | 2.68 | 12.10 | 2.61 | 1.62 | 51.0 | 27.4 |
| Tepe | Long Term, **NPV** | Triple Francis | 1.47–1.47–4.50 | 4.06 | 15.28 | 3.15 | 1.58 | 53.2 | 27.0 |
| Tepe | $N$ = 100, **MR** | Triple Francis | 1.20–2.71–2.71 | 3.62 | 14.43 | 3.08 | 1.61 | 56 | 28.0 |
| Tepe | $N$ = 100, **MR*** | Dual Francis | 1.79–4.66 | 3.52 | 14.02 | 2.93 | 1.59 | 55.2 | 28.0 |
| Tepe | $N$ = 100, **BC** | Dual Francis | 1.47–3.42 | 2.67 | 12.07 | 2.60 | 1.62 | 51.6 | 27.2 |
| Tepe | $N$ = 100, **NPV** | Triple Francis | 1.41–1.41–4.61 | 4.06 | 15.34 | 2.90 | 1.50 | 53.8 | 27.4 |
| Karacay | Long Term, **MR** | Dual Pelton | 0.60–1.60 | 2.52 | 7.67 | 1.35 | 1.46 | 44.4 | 25.4 |
| Karacay | Long Term, **BC** | Dual Pelton | 0.52–1.35 | 2.10 | 6.83 | 1.24 | 1.47 | 42.0 | 25.4 |
| Karacay | Long Term, **NPV** | Dual Pelton | 0.67–1.77 | 2.82 | 8.19 | 1.39 | 1.43 | 43.4 | 24.6 |
| Karacay | $N$ = 100, **MR** | Dual Pelton | 0.64–1.71 | 2.71 | 8.01 | 1.38 | 1.44 | 47.0 | 27 |
| Karacay | $N$ = 100, **BC** | Dual Pelton | 0.53–1.34 | 2.10 | 6.84 | 1.24 | 1.47 | 45.6 | 26.6 |
| Karacay | $N$ = 100, **NPV** | Dual Pelton | 0.68–1.79 | 2.87 | 8.28 | 1.39 | 1.42 | 46.6 | 26.2 |
| Kaplan | Long Term, **MR** | Dual Pelton | 0.62–1.23 | 3.33 | 11.53 | 2.62 | 1.68 | 42.6 | 28.8 |
| Kaplan | Long Term, **BC** | Dual Pelton | 0.47–0.85 | 2.33 | 9.91 | 2.34 | 1.72 | 37.4 | 25.4 |
| Kaplan | Long Term, **NPV** | Dual Pelton | 0.66–1.34 | 3.61 | 11.93 | 2.66 | 1.65 | 42.6 | 29 |
| Kaplan | $N$ = 100, **MR** | Dual Pelton | 0.64–1.22 | 3.33 | 11.53 | 2.63 | 1.68 | 49.6 | 29.4 |
| Kaplan | $N$ = 100, **BC** | Dual Pelton | 0.46–0.86 | 2.37 | 9.98 | 2.36 | 1.73 | 41.2 | 25.8 |
| Kaplan | $N$ = 100, **NPV** | Dual Pelton | 0.66–1.33 | 3.60 | 11.91 | 2.66 | 1.66 | 49.0 | 29.6 |

50 sampled points in each case study. The runtime for optimization and assessing robustness, varies between 26 and 35 h for a single case. Note this represents the final version of our study, following several runs with a comparable computational effort for each site. However, when using $N$ = 100 sampled points, the runtime is significantly reduced to less than 2.5 h in all the cases. In other words, the computational cost is reduced by more than 92% in each case. For more detailed information on runtime, please refer to Table 7 in the appendix.

## 6. Summary and conclusion

In this study, we introduced the HYPER-FORD, which encompasses two key innovations in the design of RoR hydropower plants. First, the $HYPER_{OP}$ module builds operational tables that integrate optimized operations to design. Second, our approximation of the FDC with a regular sampling of the FDC builds upon $HYPER_{OP}$ to enhance computational efficiency through strategic reduction of data inputs. Our

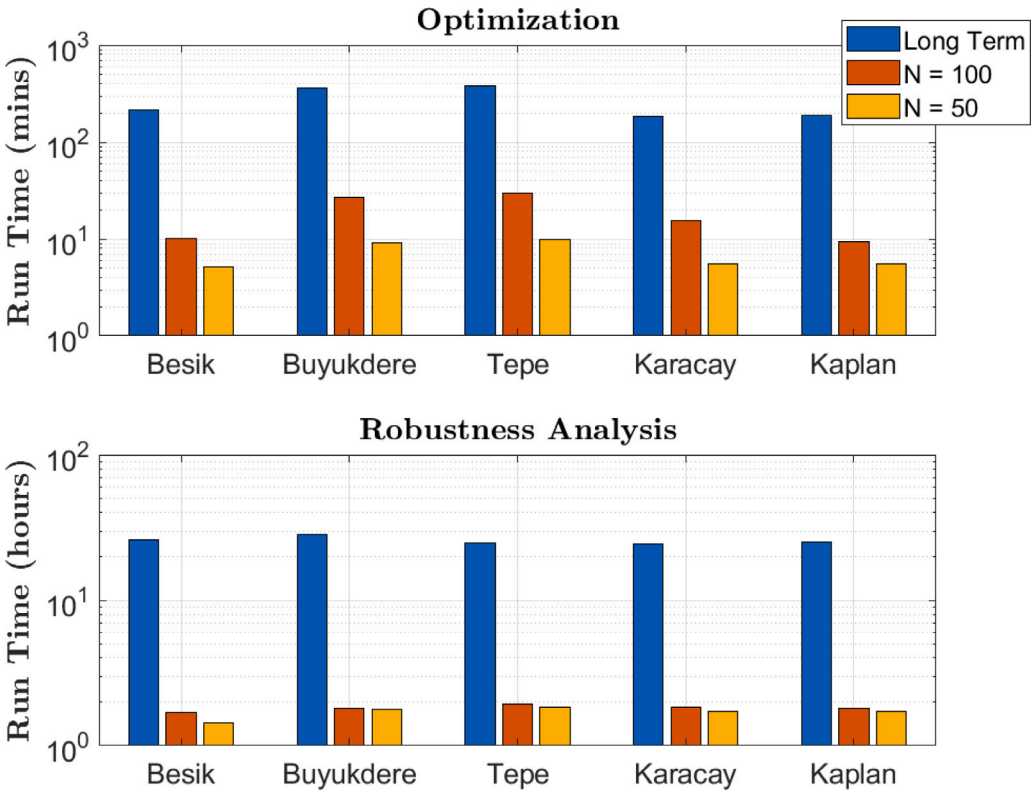


**Fig. 10.** Optimization and robustness analysis run times for long term discharge records, $N = 100$ and $N = 50$ sampling points. Note that the $y$-axis is on a logarithmic scale. The $y$-axis is on a logarithmic scale in both panels.

findings show $\text{HYPER}_{OP}$ is able to increase electricity generation by about 2% compared with traditional operational rules. Our results also demonstrate the capability of the $\text{HYPER}_{OP}$ to find design solutions not traditionally considered in engineering design of RoR hydropower plants, showing how optimized operations can expand design options.

The performance of using the FDC approximation instead of long-term daily data during optimization (of coupled design and operations) increases at very low sample sizes but stabilizes at around 100 sampled points. Beyond that, the proposed method yields a similar performance and diversity of design solutions as when using the long-term daily FDC as input. What is more, over 80% of these solutions remain Pareto optimal when re-evaluated using the long term record. This demonstrates the performance of the approach, which also slashes computational costs by 95%. Additionally, the robustness analysis indicates that modeling plausible futures using FDC approximations with 50 sampled points or more provides a reliable approximation across the entire range of design alternatives for both robustness metrics, in the sense that robustness values are close and crucially, the relative ranking of the design alternatives is well-preserved by the sampling approximation. In the coupled design optimization and robustness analysis using 100-point FDC approximations in both steps, findings demonstrate that despite the potential loss of discharge information affecting financial and robustness metrics, the impact on the generation and evaluation of key robust design alternatives is almost non-existent. Indeed, the design characteristics, such as turbine configuration (type and number), and the total installed capacity, remain consistent across the best NPV, best BC and MR alternatives for all the presented cases. In addition, while the runtime for optimization and assessing robustness, based on using long-term records, varies between 26 and 35 h for a single case, this duration significantly decreases when using FDC sampling. Specifically, the runtime is reduced to less than 2.5 h for N=100 sampled points in all cases. This represents a remarkable reduction in computational cost by more than 92% across each case.

Overall, our method strategically reduces data inputs on FDCs while preserving the gains made thanks to operations optimization. HYPER-FORD facilitates rapid analysis, optimization, and assessment of potential designs. In other words, it makes robust design and analysis more accessible. This empowers engineers and decision-makers to make informed choices, leading to the design and operation of RoR hydropower plants that are technically optimal and robust to uncertain futures. Additionally, HYPER-FORD makes the computation more sustainable by minimizing the need for high-performance computing, and by reducing carbon emissions from data centers.

Yet, while the cost-effective approach introduced here is versatile and applicable to various hydro sites, the numerical results presented in the preceding sections are limited to just five proposed cases within the same country. Although Turkey offers favorable topography for hydropower development, and experiences diverse climates, the effectiveness of this methodology should be demonstrated on other RoR hydropower plants located in regions with different topographical and hydrological characteristics to establish its general applicability. It is fitting then that HYPER-FORD makes the application of optimization and robustness analysis to a large number of cases computationally affordable. Hydropower projects are typically designed using traditional assessments that rely on historical flows by ignoring the impacts of future uncertainties (Bertoni et al., 2019). Under these conditions, optimization of these plants is based on cost–benefit analysis, generally maximizing NPV (Yildiz and Vrugt, 2019), aiming to identify the optimal solution rather than robust alternatives capable of performing well under a range of uncertain conditions. Additionally, the design and operation of these plants are often treated separately, overlooking the integration of turbine system design (e.g., Taner et al., 2017; Ray et al., 2018; Bertoni et al., 2019; Hurford et al., 2020; Bertoni et al., 2021). which is governed by site hydrology and financial constraints. Future studies, thus, should apply this methodology to hundreds of existing and potential RoR sites across wide regions, to more accurately assess the potential of small hydropower in an uncertain world.

This study, along with Yildiz et al. (2024), underscores the importance of considering turbine efficiency in hydropower plant design. By 2030, around one-fifth of the installed hydropower turbines, totaling approximately 154 GW globally (IEA, 2021), will exceed 55 years in age. Many of these turbines requiring replacement to maintain high plant performance (Brown et al., 2024), and this will lead to opportunities to retrofit hydropower plants to improve their flexibility and to adapt to changing and variable hydrological conditions. The necessity for a well-defined methodology to effectively evaluate and select the most appropriate turbine replacement or upgrade options is evident across both RoR and reservoir-based hydropower plants. To address these needs, the innovations of HYPER-FORD proposed here could be utilized for RoR retrofit effectively and expanded to encompass turbine system optimization for the design and retrofit of reservoir-based hydropower plants. The multipurpose nature of many reservoirs and their ability to buffer hydrological variability and drought – at the expense of varying hydraulic heads – present significant challenges that this latter extension of the HYPER-FORD approach will need to address.

## CRediT authorship contribution statement

**Veysel Yildiz:** Writing – original draft, Visualization, Validation, Software, Methodology, Investigation, Formal analysis, Conceptualization. **Solomon Brown:** Writing – review & editing, Supervision. **Charles Rougé:** Writing – review & editing, Visualization, Validation, Supervision, Conceptualization.

## Declaration of competing interest

The authors declare that they have no known competing financial interests or personal relationships that could have appeared to influence the work reported in this paper.

## Data availability

The HYPER-FORD methodology, along with all relevant data for the five case studies–including site and flow characteristics–is openly accessible via the University of Sheffield's data repository at https://doi.org/10.15131/shef.data.25676967.v1. Additionally, the complete methodologies and data are available on GitHub at https://github.com/Veysel-Yildiz/Robust-and-computationally-efficient-Design-for-RoR-the-HYPER-FORD.The repository includes detailed instructions to fully reproduce the experiments conducted in this study.

## Acknowledgments

Dr Charles Rougé is supported by the UK Engineering and Physical Sciences Research Council through the ' Flexible design and operation of water resource systems to tackle the triple challenge of climate change, the energy transition, and population growth' project (Ref: EP/X009459/1). Prof. Solomon Brown is supported by the UK Engineering and Physical Sciences Research Council (EPSRC) through the 'Table Top Manufacturing of Tailored Silica for Personalised Medicine [SiPM]' project (Ref: EP/V051458/1).

## Appendix

See Table 6 and Table 7

**Table 6**
Run times for robustness analysis conducted with long-term discharge data and varying sample sizes ($N$ = 10, 25, 50, 100, 200, and 500).

| Number of Points | Run time (hours) |
|---|---|
| 10 | 0.81 |
| 25 | 1.45 |
| 50 | 1.61 |
| 100 | 1.69 |
| 200 | 1.81 |
| 500 | 2.10 |
| Long Term | 26.32 |

**Table 7**
Run times for optimization and robustness analysis using long-term discharge records, comparing scenarios with $N = 100$ and $N = 50$ sampling points.

| Case Study | Long Term | $N = 100$ | $N = 50$ |
|---|---|---|---|
| Besik, optimization [minutes] | 216.9 | 10.2 | 5.2 |
| Buyukdere, optimization [minutes] | 360.5 | 27.2 | 9.2 |
| Tepe, optimization [minutes] | 384.1 | 29.4 | 9.8 |
| Karacay, optimization [minutes] | 186.2 | 15.5 | 5.5 |
| Kaplan, optimization [minutes] | 191.3 | 9.5 | 5.5 |
| Besik, robustness analysis [hours] | 26.32 | 1.69 | 1.43 |
| Buyukdere, robustness analysis [hours] | 28.29 | 1.82 | 1.78 |
| Tepe, robustness analysis [hours] | 24.65 | 1.94 | 1.83 |
| Karacay, robustness analysis [hours] | 24.52 | 1.83 | 1.71 |
| Kaplan, robustness analysis [hours] | 25.45 | 1.81 | 1.72 |

## References

Ak, M., Kentel, E., Kucukali, S., 2017. A fuzzy logic tool to evaluate low-head hydropower technologies at the outlet of wastewater treatment plants. Renew. Sustain. Energy Rev. 68, 727–737.

Alonso-Tristán, C., González-Peña, D., Díez-Mediavilla, M., Rodríguez-Amigo, M., García-Calderón, T., 2011. Small hydropower plants in Spain: A case study. Renew. Sustain. Energy Rev. 15 (6), 2729–2735.

Anagnostopoulos, J.S., Papantonis, D.E., 2007. Optimal sizing of a run-of-river small hydropower plant. Energy Convers. Manage. 48 (10), 2663–2670.

Ault, T.R., 2020. On the essentials of drought in a changing climate. Science 368 (6488), 256–260.

Basso, S., Botter, G., 2012. Streamflow variability and optimal capacity of run-of-river hydropower plants. Water Resour. Res. 48 (10).

Beck, H.E., Zimmermann, N.E., McVicar, T.R., Vergopolan, N., Berg, A., Wood, E.F., 2018. Present and future Köppen-Geiger climate classification maps at 1-km resolution. Sci. Data 5 (1), 1–12.

Bejarano, M.D., Sordo-Ward, A., Gabriel-Martin, I., Garrote, L., 2019. Tradeoff between economic and environmental costs and benefits of hydropower production at run-of-river-diversion schemes under different environmental flows scenarios. J. Hydrol. 572, 790–804.

Bertoni, F., Castelletti, A., Giuliani, M., Reed, P., 2019. Discovering dependencies, trade-offs, and robustness in joint dam design and operation: An ex-post assessment of the kariba dam. Earth's Future 7 (12), 1367–1390.

Bertoni, F., Giuliani, M., Castelletti, A., Reed, P., 2021. Designing with information feedbacks: Forecast informed reservoir sizing and operation. Water Resour. Res. 57 (3), e2020WR028112.

Bharany, S., Sharma, S., Khalaf, O.I., Abdulsahib, G.M., Al Humaimeedy, A.S., Aldhyani, T.H., Maashi, M., Alkahtani, H., 2022. A systematic survey on energy-efficient techniques in sustainable cloud computing. Sustainability 14 (10), 6256.

Blank, J., Deb, K., 2020. Pymoo: Multi-objective optimization in python. IEEE Access 8, 89497–89509.

Brown, C., Ghile, Y., Laverty, M., Li, K., 2012. Decision scaling: Linking bottom-up vulnerability analysis with climate projections in the water sector. Water Resour. Res. 48 (9), http://dx.doi.org/10.1029/2011WR011212.

Brown, S., Yildiz, V., Rougé, C., 2024. Modernising RoR Hydropower: A Study on Retrofitting Aged Turbines for Optimal Performance. Technical Report, Copernicus Meetings.

Bryant, B.P., Lempert, R.J., 2010. Thinking inside the box: A participatory, computer-assisted approach to scenario discovery. Technol. Forecast. Soc. Change 77 (1), 34–49.

Cao, Z., Zhou, X., Hu, H., Wang, Z., Wen, Y., 2022. Toward a systematic survey for carbon neutral data centers. IEEE Commun. Surv. Tutor. 24 (2), 895–936.

Cook, B.I., Mankin, J.S., Marvel, K., Williams, A.P., Smerdon, J.E., Anchukaitis, K.J., 2020. Twenty-first century drought projections in the CMIP6 forcing scenarios. Earth's Future 8 (6), e2019EF001461.

Couto, T.B., Olden, J.D., 2018. Global proliferation of small hydropower plants–science and policy. Front. Ecol. Environ. 16 (2), 91–100.

Dorber, M., Arvesen, A., Gernaat, D., Verones, F., 2020. Controlling biodiversity impacts of future global hydropower reservoirs by strategic site selection. Sci. Rep. 10 (1), 1–13.

Fang, Z., Zhang, W., Brandt, M., Abdi, A.M., Fensholt, R., 2022. Globally increasing atmospheric aridity over the 21st century. Earth's Future 10 (10), e2022EF003019.

Gernaat, D.E., Bogaart, P.W., van Vuuren, D.P., Biemans, H., Niessink, R., 2017. High-resolution assessment of global technical and economic hydropower potential. Nature Energy 2 (10), 821–828.

Gielen, D., Boshell, F., Saygin, D., Bazilian, M.D., Wagner, N., Gorini, R., 2019. The role of renewable energy in the global energy transformation. Energy Strategy Rev. 24, 38–50.

Girma, Z., 2016. Techno-economic feasibility of small scale hydropower in Ethiopia: The case of the Kulfo River, in Southern Ethiopia. J. Renew. Energy 2016.

Giuliani, M., Castelletti, A., 2016. Is robustness really robust? How different definitions of robustness impact decision-making under climate change. Clim. Change 135 (3–4), 409–424.

Haasnoot, M., Kwakkel, J.H., Walker, W.E., ter Maat, J., 2013. Dynamic adaptive policy pathways: A method for crafting robust decisions for a deeply uncertain world. Glob. Environ. Change 23 (2), 485–498. http://dx.doi.org/10.1016/j.gloenvcha.2012.12.006.

Hadka, D., Reed, P., 2012. Diagnostic assessment of search controls and failure modes in many-objective evolutionary optimization. Evol. Comput. 20 (3), 423–452.

Herman, J.D., Reed, P.M., Zeff, H.B., Characklis, G.W., 2015. How should robustness be defined for water systems planning under change? J. Water Resour. Plan. Manag. 141 (10), 04015012. http://dx.doi.org/10.1061/(ASCE)WR.1943-5452.0000509.

Herman, J.D., Zeff, H.B., Reed, P.M., Characklis, G.W., 2014. Beyond optimality: Multistakeholder robustness tradeoffs for regional water portfolio planning under deep uncertainty. Water Resour. Res. 50 (10), 7692–7713. http://dx.doi.org/10.1002/2014WR015338.

Hernandez, L., Jimenez, G., Marchena, P., 2018. Energy efficiency metrics of university data centers. Knowl. Eng. Data Sci. 1 (2), 64–73.

Hurford, A., Harou, J.J., Bonzanigo, L., Ray, P., Karki, P., Bharati, L., Chinnasamy, P., 2020. Efficient and robust hydropower system design under uncertainty-A demonstration in Nepal. Renew. Sustain. Energy Rev. 132, 109910.

Hussain, S.M., Wahid, A., Shah, M.A., Akhunzada, A., Khan, F., Amin, N.u., Arshad, S., Ali, I., 2019. Seven pillars to achieve energy efficiency in high-performance computing data centers. Recent Trends Adv. Wirel. IoT-enabled Netw. 93–105.

IEA, 2021. Hydropower Special Market Report. International Energy Agency, Paris, [Accessed 18 May 2023].

Ishibuchi, H., Imada, R., Setoguchi, Y., Nojima, Y., 2018. How to specify a reference point in hypervolume calculation for fair performance comparison. Evol. Comput. 26 (3), 411–440.

Jones, N., 2018. How to stop data centres from gobbling up the world's electricity. Nature 561 (7722), 163–166.

Kasprzyk, J.R., Nataraj, S., Reed, P.M., Lempert, R.J., 2013. Many objective robust decision making for complex environmental systems undergoing change. Environ. Model. Softw. 42, 55–71. http://dx.doi.org/10.1016/j.envsoft.2012.12.007.

Katal, A., Dahiya, S., Choudhury, T., 2022. Energy efficiency in cloud computing data centers: a survey on software technologies. Cluster Comput. 1–31.

Katal, A., Dahiya, S., Choudhury, T., 2023. Energy efficiency in cloud computing data centers: a survey on software technologies. Cluster Comput. 26 (3), 1845–1875.

Kishore, T.S., Patro, E.R., Harish, V., Haghighi, A.T., 2021. A comprehensive study on the recent progress and trends in development of small hydropower projects. Energies 14 (10), 2882.

Kuriqi, A., Pinheiro, A.N., Sordo-Ward, A., Garrote, L., 2020. Water-energy-ecosystem nexus: Balancing competing interests at a run-of-river hydropower plant coupling a hydrologic–ecohydraulic approach. Energy Convers. Manage. 223, 113267.

Kwakkel, J.H., Walker, W.E., Haasnoot, M., 2016. Coping with the wickedness of public policy problems: approaches for decision making under deep uncertainty. J. Water Resour. Plan. Manag. 142 (3), 01816001.

Lannelongue, L., Grealey, J., Inouye, M., 2021. Green algorithms: quantifying the carbon footprint of computation. Adv. Sci. 8 (12), 2100707.

Lempert, R.J., 2002. A new decision sciences for complex systems. Proc. Natl. Acad. Sci. 99 (suppl 3), 7309–7313. http://dx.doi.org/10.1073/pnas.082081699.

Mamo, G., Marence, M., Chacon-Hurtado, J., Franca, M., 2018. Optimization of run-of-river hydropower plant capacity. Int. Water Power Dam Constr.

McCollum, D., Gomez Echeverri, L., Riahi, K., Parkinson, S., 2017. Sdg7: Ensure Access to Affordable, Reliable, Sustainable and Modern Energy for All. International Council for Science, Paris.

McPhail, C., Maier, H., Kwakkel, J., Giuliani, M., Castelletti, A., Westra, S., 2018. Robustness metrics: How are they calculated, when should they be used and why do they give different results? Earth's Future 6 (2), 169–191.

Moran, E.F., Lopez, M.C., Moore, N., Müller, N., Hyndman, D.W., 2018. Sustainable hydropower in the 21st century. Proc. Natl. Acad. Sci. 115 (47), 11891–11898.

Pokhrel, Y., Burbano, M., Roush, J., Kang, H., Sridhar, V., Hyndman, D.W., 2018. A review of the integrated effects of changing climate, land use, and dams on Mekong river hydrology. Water 10 (3), 266.

Quinn, J.D., Reed, P.M., Giuliani, M., Castelletti, A., 2017. Rival framings: A framework for discovering how problem formulation uncertainties shape risk management trade-offs in water resources systems. Water Resour. Res. 53 (8), 7208–7233.

Quinn, J.D., Reed, P.M., Giuliani, M., Castelletti, A., Oyler, J.W., Nicholas, R.E., 2018. Exploring how changing monsoonal dynamics and human pressures challenge multireservoir management for flood protection, hydropower production, and agricultural water supply. Water Resour. Res. 54 (7), 4638–4662. http://dx.doi.org/10.1029/2018WR022743.

Ray, P.A., Bonzanigo, L., Wi, S., Yang, Y.C.E., Karki, P., Garcia, L.E., Rodriguez, D.J., Brown, C.M., 2018. Multidimensional stress test for hydropower investments facing climate, geophysical and financial uncertainty. Global Environ. Change 48, 168–181. http://dx.doi.org/10.1016/j.gloenvcha.2017.11.013.

Reed, P.M., Hadka, D., Herman, J.D., Kasprzyk, J.R., Kollat, J.B., 2013. Evolutionary multiobjective optimization in water resources: The past, present, and future. Adv. Water Resour. 51, 438–456.

Sadegh, M., Vrugt, J., Gupta, H.V., Xu, C., 2016. The soil water characteristic as new class of closed-form parametric expressions for the flow duration curve. J. Hydrol. 535, 438–456.

Salazar, J.Z., Reed, P.M., Herman, J.D., Giuliani, M., Castelletti, A., 2016. A diagnostic assessment of evolutionary algorithms for multi-objective surface water reservoir control. Adv. Water Resour. 92, 172–185.

Santolin, A., Cavazzini, G., Pavesi, G., Ardizzon, G., Rossetti, A., 2011. Techno-economical method for the capacity sizing of a small hydropower plant. Energy Convers. Manage. 52 (7), 2533–2541.

Shaktawat, A., Vadhera, S., 2021. Risk management of hydropower projects for sustainable development: a review. Environ. Dev. Sustain. 23 (1), 45–76.

Spinoni, J., Naumann, G., Carrao, H., Barbosa, P., Vogt, J., 2014. World drought frequency, duration, and severity for 1951–2010. Int. J. Climatol. 34 (8), 2792–2804.

Spinoni, J., Vogt, J.V., Naumann, G., Barbosa, P., Dosio, A., 2018. Will drought events become more frequent and severe in Europe? Int. J. Climatol. 38 (4), 1718–1736.

Sreeparvathy, V., Srinivas, V., 2022. Meteorological flash droughts risk projections based on CMIP6 climate change scenarios. npj Clim. Atmos. Sci. 5 (1), 77.

Taner, M.Ü., Ray, P., Brown, C., 2017. Robustness-based evaluation of hydropower infrastructure design under climate change. Clim. Risk Manag. 18, 34–50.

Tsuanyo, D., Amougou, B., Aziz, A., Nka Nnomo, B., Fioriti, D., Kenfack, J., 2023. Design models for small run-of-river hydropower plants: a review. Renew. Wind Water Sol. 10 (1), 3.

UNIDO, 2022. World Small Hydropower Development Report. United Nations Industrial Development Organization (UNIDO) and the International Center on Small Hydro Power (ICSHP), URL: https://www.unido.org/WSHPDR2022.

Van Veldhuizen, D.A., 1999. Multiobjective Evolutionary Algorithms: Classifications, Analyses, and New Innovations. Air Force Institute of Technology.

Vogel, R.M., Fennessey, N., 1994. Flow duration curves I: new interpretation and confidence intervals. J. Water Resour. Plan. Manag. 120 (4).

Vrugt, J.A., Robinson, B.A., 2007. Improved evolutionary optimization from genetically adaptive multimethod search. Proc. Natl. Acad. Sci. 104 (3), 708–711. http://dx.doi.org/10.1073/pnas.0610471104, URL: https://www.pnas.org/content/104/3/708, arXiv:https://www.pnas.org/content/104/3/708.full.pdf.

Winemiller, K.O., McIntyre, P.B., Castello, L., Fluet-Chouinard, E., Giarrizzo, T., Nam, S., Baird, I.G., Darwall, W., Lujan, N.K., Harrison, I., Stiassny, M.L.J., Silvano, R.A.M., Fitzgerald, D.B., Pelicice, F.M., Agostinho, A.A., Gomes, L.C., Albert, J.S., Baran, E., Petrere, M., Zarfl, C., Mulligan, M., Sullivan, J.P., Arantes, C.C., Sousa, L.M., Koning, A.A., Hoeinghaus, D.J., Sabaj, M., Lundberg, J.G., Armbruster, J., Thieme, M.L., Petry, P., Zuanon, J., Vilara, G.T., Snoeks, J., Ou, C., Rainboth, W., Pavanelli, C.S., Akama, A., van Soesbergen, A., Sáenz, L., 2016. Balancing hydropower and biodiversity in the Amazon, Congo, and Mekong. Science 351 (6269), 128–129. http://dx.doi.org/10.1126/science.aac7082, URL: https://www.science.org/doi/abs/10.1126/science.aac7082, arXiv:https://www.science.org/doi/pdf/10.1126/science.aac7082.

Yildiz, V., Brown, S., Rougé, C., 2024. Importance of variable turbine efficiency in run-of-river hydropower design under deep uncertainty. Water Resour. Res. 60 (6), e2023WR035713.

Yildiz, V., Hatipoglu, M.A., Kumcu, S.Y., 2022. Climate change impacts on water resources. In: Water and Wastewater Management: Global Problems and Measures. Springer International Publishing, Cham, pp. 17–25. http://dx.doi.org/10.1007/978-3-030-95288-4_2.

Yildiz, V., Milton, R., Brown, S., Rougé, C., 2023. Technical note: Statistical generation of climate-perturbed flow duration curves. Hydrol. Earth Syst. Sci. 27 (13), 2499–2507. http://dx.doi.org/10.5194/hess-27-2499-2023, URL: https://hess.copernicus.org/articles/27/2499/2023/.

Yildiz, V., Vrugt, J.A., 2019. A toolbox for the optimal design of run-of-river hydropower plants. Environ. Model. Softw. 111, 134–152. http://dx.doi.org/10.1016/j.envsoft.2018.08.018.

Yilmaz, K.K., Gupta, H.V., Wagener, T., 2008. A process-based diagnostic approach to model evaluation: Application to the NWS distributed hydrologic model. Water Resour. Res. 44 (9), http://dx.doi.org/10.1029/2007WR006716.

Zarfl, C., Lumsdon, A.E., Berlekamp, J., Tydecks, L., Tockner, K., 2015. A global boom in hydropower dam construction. Aquat. Sci. 77, 161–170.

Zhang, Y., Zheng, H., Zhang, X., Leung, L.R., Liu, C., Zheng, C., Guo, Y., Chiew, F.H., Post, D., Kong, D., et al., 2023. Future global streamflow declines are probably more severe than previously estimated. Nature Water 1 (3), 261–271.

Zitzler, E., Thiele, L., Laumanns, M., Fonseca, C.M., Da Fonseca, V.G., 2003. Performance assessment of multiobjective optimizers: An analysis and review. IEEE Trans. Evol. Comput. 7 (2), 117–132.